RESEARCH PAPER

Channels 5:6, 1-1; November/December 2011; © 2011 Landes Bioscience

Residual Cx45 and its relationship to Cx43 in Murine ventricular myocardium

Mingwei Bao,[1,†] Evelyn M. Kanter,[1] Richard Y.C. Huang,[2] Stephan Maxeiner,[5,‡] Marina Frank,[5] Yan Zhang,[1] Richard B. Schuessler,[3] Timothy W. Smith,[1] R. Reid Townsend,[1,4] Henry W. Rohrs,[2] Viviana M. Berthoud,[6] Klaus Willecke,[5] James G. Laing[1] and Kathryn A. Yamada[1,*]

[1]Department of Medicine; [2]Chemistry; [3]Surgery; [4]Cell Biology and Physiology; Washington University School of Medicine; St. Louis, MO; [5]Institute of Genetics; University of Bonn; Bonn, Germany; [6]Department of Pediatrics; University of Chicago; Chicago, IL USA

[†]Current Affiliation: Department of Cardiology; Renmin Hospital of Wuhan University; Wuhan, Hubei China; [‡]Neurosciences Institute; Stanford School of Medicine; Palo Alto, CA USA

Key words: connexin45, gap junctions, quantitative immunoblots, co-immunoprecipitation, electron microscopy, Cx45 phosphorylation, CaMKII, transgenic mice

Abbreviations: Cx, connexin; Cx45, connexin45; Cx43, connexin43; Cx30.2, connexin30.2; Cx31.9, connexin31.9; Cx40, connexin40; GST, glutathione S-transferase; CaMKII, Ca^{2+}/calmodulin-dependent protein kinase II; CK1, casein kinase 1; WT, wild-type; Cx45OEs, mice with cardiac-selective overexpression of Cx45; LV, left ventricular; RV, right ventricular; AV, atrio-ventricular; SA, sino-atrial; PCR, polymerase chain reaction; α-MHC, alpha-myosin heavy chain; fl, floxed; $Cx40^{KICx45/KICx45}$, Cx40 knockin Cx45 mice; CT, carboxy-terminal; MS, mass spectrometry; SDS, sodium dodecyl sulfate; IB, immunoblotting

Gap junction channels in ventricular myocardium are required for electrical and metabolic coupling between cardiac myocytes and for normal cardiac pump function. Although much is known about expression patterns and remodeling of cardiac connexin (Cx)43, little is known about the less abundant Cx45, which is required for embryonic development and viability, is downregulated in adult hearts, and is pathophysiologically upregulated in human end-stage heart failure. We applied quantitative immunoblotting and immunoprecipitation to native myocardial extracts, immunogold electron microscopy to cardiac tissue and membrane sections, electrophysiological recordings to whole hearts, and high-resolution tandem mass spectrometry to Cx45 fusion protein, and developed two new tools, anti-Cx45 antisera and Cre^{+};Cx45 floxed mice, to facilitate characterization of Cx45 in adult mammalian hearts.

We found that Cx45 represents 0.3% of total Cx protein (predominantly 200 fmol Cx43 protein/μg ventricular protein) and colocalizes with Cx43 in native ventricular gap junctions, particularly in the apex and septum. Cre^{+};Cx45 floxed mice express 85% less Cx45, but do not exhibit overt electrophysiologic abnormalities. Although the basal phosphorylation status of native Cx45 remains unknown, CaMKII phosphorylates eight Ser/Thr residues in Cx45 in vitro.

Thus, although downregulation of Cx45 does not produce notable deficits in electrical conduction in adult, disease-free hearts, Cx45 is a target of the multifunctional kinase CaMKII, and the phosphorylation status of Cx45 and the role of Cx43/Cx45 heteromeric gap junction channels in both normal and diseased hearts merits further investigation.

Supplementary Material

*Correspondence to: Kathryn A. Yamada; Email: kyamada@wustl.edu
Submitted: 07/19/11; Revised: 10/24/11; Accepted: 10/25/11
http://dx.doi.org

Supplemental Materials and Methods

Gap Junction-Enriched Membrane Preparations

Gap junction-enriched membrane fractions were prepared using a procedure published by Kensler and Goodenough,[1] but in the presence of 1 mM phenylmethylsulfonyl fluoride (PMSF) to avoid proteolysis of connexins as demonstrated by Manjunath et al.[2] Briefly, ventricular tissue was homogenized with a Dremel Tissue Tearor in 1mM $NaHCO_3$ buffer (pH 8.2) containing 1 mM PMSF and spun at 2000×g for 20 min at 5°C (Sorvall SA-600 rotor, 3700 rpm). The pellets were resuspended in 0.6 M KI in a 6 mM $Na_2S_2O_3$ buffer and stirred overnight. The next day, the solution was pelleted and resuspended in 0.6 M KI in 6 mM $Na_2S_2O_3$ plus 5 mM Tris buffer (Tris-KI, pH 9) and spun at 22,700×g for 30 min at 5°C (Sorvall SA-600 rotor, 12,500 rpm). The KI-insoluble pellets were resuspended in 50% sucrose in Tris-KI using a Tissue Tearor and Cole Parmer sonicator, and spun in a 45%/35%/30% step gradient at 109,900×g for 2 hr at 5°C using a Beckman Optima MAX-E ultracentrifuge. The fraction floating on the 30% sucrose layer was collected and diluted in 5 mM Tris buffer (pH 9) and spun at 109,900×g for 30 min at 5°C. The pellets were resuspended in 5 mM Tris buffer (pH 9) using a Wheaton Dounce homogenizer and dialyzed overnight against 5 mM Tris buffer at 4°C to remove residual KI. The dialysate was spun at 16,100×g for 40 min at 4°C in an Eppendorf microcentrifuge. The pellets were resuspended in 0.5% Tween 20 in 5 mM Tris buffer (pH 10), layered on a 43%/30% sucrose step gradient and spun at 109,900×g for 1.5 hr at 15°C. Partially purified gap junctions were obtained from the 43%/30% interface, spun down at 109,900×g for 30 min at 15°C, resuspended in 0.3% deoxycholate, layered on another 43%/30% sucrose step gradient, spun again at 109,900×g for 1.5 hr at 15°C. The material at the 43%/30% interface was collected, diluted in 5 mM Tris buffer

(pH 10) and spun at 109,900×g for 30 min at 5°C to yield the final gap junction-enriched fraction with an approximate yield of 3-9 µg protein per g of heart (wet weight).

Quantitative Immunoblot Analysis

BL21-CodonPlus competent cells (Stratagene cat. #230280) were transformed with a construct encoding GST (in pGEX-2T, GE Healthcare/Amersham Biosciencs cat. #28-9546-53) followed by amino acids 237-382 of the carboxyl terminus (CT) of rat Cx43 (GST-Cx43 CT, MW 42,122 g/mol) or a construct encoding a 6 His-epitope (in pET-15b, EMD Chemicals/Novagen cat. #69661-3) followed by amino acids 259-396 of the CT of mouse Cx45 (6 His-Cx45 CT, MW 16,356 g/mol), a generous gift from Dr. Thomas Steinberg. The GST-Cx43 CT fusion protein was purified using a B-PER GST Fusion Protein Purification Kit (Thermo Scientific/Pierce cat. #78200). In some experiments, the GST domain of the protein was removed by treating the purified fusion protein with thrombin (80 units/mL, GE Bioscience cat. #27-0846-01) overnight at 4ºC. GST was removed from the digest by fractionation over an immobilized glutathione agarose column included in the kit. Cx43 CT was dialyzed against Tris-buffered saline for 48 hr. The 6 His-Cx45 CT fusion protein was purified using a B-PER 6xHis Fusion Protein Purification Kit (Thermo Scientific/Pierce cat. #78100). The cells were lysed in 8 M urea in Tris buffer, pH 8. The lysates were clarified by centrifugation and the supernatants were passed over a Nickel Chelated agarose column included in the kit. The column was washed with 8 M urea, pH 6.3, and eluted with 8 M urea, pH 4.5. The fusion protein was concentrated in a Centricon Ultracel YM-3 centrifugal filter (Millipore) at 4350 x g overnight, then dialyzed against Tris-buffered saline for 48 hr. Protein determinations were made using a Micro BCA protein assay (Thermo Scientific/Pierce cat. #23235).

Three major challenges became evident during our quantitative immunoblot experiments. First, despite taking great care in the production of connexin fusion proteins and in protein determinations, there was unavoidable variability in the standard curves obtained from different fusion protein preparations (Sup. Figure S1). Second, we were concerned that thrombin cleavage was incomplete in some preparations, contributing to variability in Cx43 CT protein yields. Thus, we decided to re-run quantitative immunoblots on 12 of the 16 cardiac samples for which we had sufficient homogenate remaining, using increasing concentrations of uncleaved GST-Cx43 CT fusion protein as standards. Third, in our initial gels, we ran ventricular tissue sample and both Cx43 CT and Cx45 CT fusion proteins in the same lane. However, GST-Cx43 CT fusion protein migrates with roughly the same electrophoretic mobility as native cardiac Cx43 (~41-45 kD). Therefore, in each of the gels used for the final quantitative immunoblot calculations, ventricular homogenates, GST-Cx43 CT and 6 His-Cx45 CT fusion proteins were each run in different lanes. Three separate Cx43 CT and three separate Cx45 CT fusion protein preparations were used in the quantitative immunoblots reported here.

Ventricular homogenates from a total of 16 hearts were run on 9 separate gels as follows. Myocardial extracts were prepared by homogenization (20 strokes) using a Duall 20 glass conical pestle (Kimble/Kontes, Vineland, NJ) and sonication (6×15 s, Cole-Parmer 8850, Cole-Parmer Instrument Co.) in a buffer solution containing: 1 mM $NaHCO_3$, 5 mM EDTA, 1 mM EGTA, pH 8.0 containing the following protease inhibitors: 1 μM pepstatin, 100 nM aprotinin, 1 mM benzamidine, 1 mM iodoacetamide, 1 μM leupeptin, 1 mM PMSF. Proteins (15 μg of ventricular homogenates) were resolved by SDS-polyacrylamide (10%) gel electrophoresis (SDS-PAGE) and transferred to nitrocellulose membranes for incubation with rabbit anti-Cx43 (1:5000, Zymed cat. #71-0700 or 1:45-48,000 Sigma cat. #C6219), protein A-purified rabbit

anti-Cx45 (1:5000, generous gift from Dr. T. Steinberg, Washington University, St. Louis, MO; or 1:5000, new anti-Cx45 antiserum produced in the present study), goat anti-actin (1:1000, Santa Cruz cat. #sc-1615), or mouse anti-GAPDH (1:5-10,000, Research Diagnostics, Inc./Fitzgerald Industries, Int. cat. #10R-G109A) primary antibodies. HRP-conjugated goat anti-rabbit (1:10,000, Jackson ImmunoResearch cat. #111-035-144), donkey anti-goat (1:20,000, Santa Cruz cat. #sc-2020), and sheep anti-mouse (1:10,000, GE Healthcare/Amersham Biosciences Corp. cat. #NA931) antibodies were used as secondary antibodies. Protein bands were visualized using Western Lightning Chemiluminescence Reagent Plus (Perkin Elmer cat. #NEL104). The intensities of the immunoreactive bands were quantified by densitometric analysis using Adobe Photoshop. Standard curves were generated in Microsoft Excel using the densitometric values of the fusion proteins. The densitometric values of the connexin bands (per 15 μg protein loaded on each gel) were interpolated in the standard curves to calculate the number of fmol of connexin/μg of protein in each tissue sample.

Immunoprecipitations

We performed co-immunoprecipitation experiments on murine ventricles that were flash frozen, pulverized, homogenized and lysed in a buffer solution containing 1.5% NP-40, 1% Triton X-100, 0.1% SDS, 0.1% BSA and protease inhibitors. Either monoclonal anti-Cx43 (Chemicon cat. #MAB3067) or monoclonal anti-Cx45 (Chemicon cat. #MAB3100) antibody was incubated with protein G sepharose (Sigma cat. #P4691) for 1 hr. The lysate was incubated with the antibody-bound beads plus protease inhibitor cocktail (Sigma cat. #P8340) for 1 hr at 4ºC to immunoprecipitate Cx43-associated and Cx45-associated proteins, respectively. A nonspecific IgG_1 (Chemicon cat. #PP100) was used as a negative control. The

immunoprecipitates (beads) were spun down in a microcentrifuge at 16,100×g for 15 min at 4ºC, washed 3× in lysis buffer with BSA, and suspended in lysis buffer without BSA plus sample buffer with β-mercaptoethanol for immunoblot analysis as described above.

Immunogold Electron Microscopy

Ventricular tissue samples cut with a vibratome and isolated gap junction-enriched membrane preparations were stained using a pre-embedding procedure described previously.[3,4] Briefly, samples were incubated in NH_4Cl for 30 min, followed by incubation in blocking buffer (EY Laboratories, Inc. cat. #2205050) for 1 hr. Samples were incubated in primary antibodies (mouse anti-Cx43 antibody, Chemicon cat. #MAB3068, 1:500 and rabbit anti-Cx45 antibody, Dr. T. Steinberg, 1:500) overnight at 4ºC. The samples were then incubated in secondary antibodies (goat anti-mouse IgG conjugated to 10 nm colloidal gold cat. #GAF-011-10 and goat anti-rabbit IgG conjugated to 20 nm colloidal gold cat. #GAF-012-20, respectively, EY Laboratories, undiluted). Samples were post-fixed in 2.5% glutaraldehyde in phosphate-buffered saline followed by 2% OsO_4, embedded in PolyBed 812 (Polysciences, Inc. cat. #08792-1), sectioned, poststained with uranyl acetate and lead citrate according to standard EM procedures, and examined with a Philips EM-200 electron microscope (Phillips Electronic Instruments).

Immunostaining and Confocal Analysis

Immunostaining. Hearts were cut in half coronally and the posterior half was frozen cut side down in O.C.T. Ten-μm frozen sections were cut and fixed in 4% paraformaldehyde. Sections were incubated in rabbit anti-Cx45 (1:200, Dr. T. Steinberg or 1:100, new affinity-purified anti-Cx45 antiserum produced in the present study), rabbit anti-Cx43 (1:400, Sigma cat.

#C6219), or goat anti-Cx40 (1:200, Santa Cruz cat. #sc-20466) antibodies at 4ºC in a humidity chamber overnight. The next day, after 3 washes in PBS, the sections were incubated in Cy3-conjugated goat anti-rabbit (1:200-1:300 for anti-Cx45, 1:300 for anti-Cx43, Jackson ImmunoResearch cat. #111-165-144) or donkey anti-goat (1:300, Jackson ImmunoResearch cat. #705-165-147) secondary antibody at room temperature for 2 h.

Confocal analysis. Sections were analyzed on a Zeiss LSM-510 META confocal microscope in the Cell Biology & Physiology Confocal Facility. The system consists of a Zeiss Axiovert 200M microscope and LSM-510 operating and image analysis software. A total of 5 Cre^{+};$Cx45^{fl/fl}$ and 8 control hearts were stained in 4 experiments. Adjacent tissue sections were stained with anti-Cx45, anti-Cx43, anti-Cx40 and secondary (alone) antibodies for each experiment. Confocal images for a given antibody and experiment were acquired on the same day with identical confocal microscope settings. For Cx45 immunostaining, 5-10 fields per heart were acquired from 4 Cre^{+};$Cx45^{fl/fl}$ and 5 control hearts. For Cx43 immunostaining, 3-10 fields per heart were acquired from 4 Cre^{+};$Cx45^{fl/fl}$ and 5 control hearts. For Cx40 immunostaining, 2-5 fields per heart were acquired from 5 Cre^{+};$Cx45^{fl/fl}$ and 8 control hearts. Immunoreactive signal was quantified by an investigator blinded to genotype using ImageJ software. Gap junction staining was defined as 5 or more contiguous pixels; signal ≤ 4 pixels was considered background or nonspecific and was not included in the quantification.

Anti-Cx45 Polyclonal Antibody Production

Cx45 C-Terminal (CT) fusion protein. The same 6 His-Cx45 CT fusion protein that was used in the quantitative immunoblots was used as antigen to immunize rabbits for production of anti-Cx45 antiserum at Pocono Rabbit Farm & Laboratory. Fusion protein was concentrated in a

Centricon filter and dialyzed as described above. Antiserum obtained from Pocono was aliquoted and affinity purified using Affi-Prep 10 Affinity Support (Bio-Rad cat. #153-0002).

Antibody characterization. We performed immunoblotting experiments on cells and tissues with varying levels of Cx45, including HeLa cells transfected to overexpress either mouse Cx45 (HeLa-45) or rat Cx43 (HeLa-43). As shown in Sup. Figure S2A, the new anti-Cx45 antiserum recognized protein extracted from HeLa-45 cells, but not from control HeLa or HeLa-43 cells. Stronger bands at 45 kD were observed in lanes loaded with protein extracted from Cx45 overexpressing compared with nontransgenic hearts and also in lanes loaded with protein extracted from Cx45 knock-in compared with wild-type atria. Furthermore, anti-Cx45 antiserum recognized bands in lanes loaded with protein extracted from wild-type embryos, but not from protein extracted from Cx45 null embryos (Sup. Figure S2B). Finally, the new anti-Cx45 antiserum demonstrated increased immunoreactive signal in ventricular tissue sections cut from Cx45 overexpressors (Sup. Figure S2C) and Cx45 knock-in atria (Sup. Figure S2D) compared with wild-type myocardium.

In vitro Electrophysiology Studies of Cardiac Cx45 Transgenic Mice

Cardiac Activation Times and Inhomogeneity Index in Cx45OEs. C57BL6 wild-type (n = 6) and Cx45OEs (n = 4) were anesthetized with Avertin (0.1 mg/kg, Sigma cat. #T48402 plus cat. #240486) for acquisition of surface ECG recordings followed by removal and retrograde perfusion of hearts via the aorta at 25ºC[5] for in vitro electrophysiology studies. Perfusion pressure was maintained between 40 and 60 mm Hg by adjusting the flow rate. One bipolar electrode (Frederick Haer cat. #PBSA-10075) was placed on the right atrium or high right septum for pacing. A second bipolar electrode was placed at the right ventricular (RV) apex for

pacing. Ventricular effective refractory periods were determined by programmed electrical stimulation in which 8 S1 paced beats (180 ms cycle length) were followed by premature S2s at decrementing cycle lengths until a ventricular signal was not captured. Di-4-ANEPPS (Molecular Probes/Invitrogen cat. #D-1199) was administered in the perfusate for multi-site optical mapping of the anterior and lateral left ventricular (LV) free walls. Blebbistatin (3.4 μM, Tocris Bioscience cat. #1760) was administered via the perfusate to inhibit cardiac contraction, thereby minimizing motion artifact. Signals were focused through a NIKKOR 50 mm lens (Nikon) and detected by a photodiode array (Hamamatsu), filtered, amplified and acquired by custom-made hardware and data acquisition and analysis software developed in the Department of Surgery at Washington University. Activation times assigned by the software were checked and manually reassigned if necessary. Inhomogeneity indices were calculated as described by Lammers et al.[6] Activation times were obtained from optical action potentials collected from the LV lateral free wall after pacing at a cycle length of either 180 ms or 130 ms. Each photodiode pair in each quadruplet of photodiodes was compared to determine the maximum difference in activation times in each quadruplet. The median and range of the maximum differences were used to calculate phase differences and inhomogeneity (variation coefficient, P_{5-95}/P_{50}) indices.

Electrophysiological Testing in Mice with Cardiac Cx45 Ablation. A total of 11 FVB controls and 4 cardiac Cx45-deficient mice were subjected to limited electrophysiological testing in vitro. Surface ECGs were recorded from 9 mice (n = 5 controls and n = 4 Cx45-deficient). Optical maps were obtained from 5 mice (n = 3 controls and n = 2 Cx45-deficient). Activation times were measured in 10 mice (n = 8 controls and n = 2 Cx45-deficient).

Mice were anesthetized for acquisition of surface ECG recordings and removal of their hearts for retrograde perfusion and administration of Di-4-ANEPPS and blebbistatin for optical

mapping as described above. For electrogram recordings, a CIB'er octapolar intracardiac catheter (NuMed) was inserted into the RV cavity and used for pacing either from the right atrium (using the proximal electrode pair) or from the RV apex (using the distal electrode pair); a bipolar electrode (Frederick Haer) was placed on the anterolateral epicardial surface and was used for recording epicardial electrograms. Activation times between the RV apex and the LV lateral free wall were calculated under 3 conditions: spontaneous rhythm, right atrial pacing at a cycle length of 180 ms, and RV apical pacing at a cycle length of 180 ms.

High-Resolution Mass Spectrometric Identification of Cx45 Phosphorylation Sites

In vitro phosphorylation of Cx45 CT by CaMKII. Cx45 CT fusion protein (8.5 – 10.5 μg) was incubated with 1.2 μmol/L calmodulin, 210 μmol/L ATP, 2 mmol/L $CaCl_2$ and 1,500 U CaMKII (New England Biolabs cat. #P6060S, per the manufacturer's instructions) at 30ºC for 24 h. The reaction was stopped on ice and phosphatase inhibitors were added at a final concentration of 1 mmol/L NaF and 2 mmol/L Na_3VO_4. Control reactions contained Cx45 CT fusion protein, calmodulin, ATP, Ca^{2+} and buffer without CaMKII. In additional experiments we used casein kinase 1 (CK1, New England Biolabs cat. #P6030S, 1,500 U, 24 h, per the manufacturer's instructions).

Protein digestion and mass spectrometry. Cx45 CT fusion protein was precipitated, resolubilized, reduced, alkylated and digested as described previously.[7] TiO_2 tips (Glygen cat. #NT3TIO) were used for phosphopeptide enrichment. Mass spectrometric analysis was performed using a Thermo LTQ Orbitrap XL with collision-induced dissociation (CID) and electron transfer dissociation (ETD) (Thermo Fisher). One parent ion scan (*m/z* 350 – 2000) (MS1) was acquired to determine 6 data-dependent, alternating CID and ETD mass spectra

(MS2). For analysis with the LTQ-FT Ultra (Thermo Fisher), one parent scan (*m/z* 350 – 2000) was used to trigger 8 data-dependent CID spectra. The raw files were processed using LCQ-DTA software (ThermoFisher) and the resulting files were exported to MASCOT 2.2.06 (Matrix Science). The NCBI nonredundant mammalian database (downloaded 20090105) was searched with the fixed modifications reported previously.[7] Identification of all phosphopeptides were verified manually. Phosphopeptides identified by MASCOT were subjected to in silico digestion using Protein Prospector MS-Digest (http://prospector.ucsf.edu/prospector/mshome.htm), theoretical MS2 spectra were generated using Protein Prospector MS-Product, and lists of theoretical fragment ions were generated. Tables of theoretical and observed fragment ions for each identified phosphopeptide are included below (Sup. Tables S5-S13). Manual comparison was used to deduce the site of each modification.

References

1. Kensler RW, Goodenough DA. Isolation of mouse myocardial gap junctions. J Cell Biol 1980;86:755-764.
2. Manjunath CK, Goings GE, Page E. Proteolysis of cardiac gap junctions during their isolation from rat hearts. J Membr Biol 1985;85:159-168.
3. Kanter HL, Laing JG, Beyer EC, Green KG, Saffitz JE. Multiple connexins colocalize in canine ventricular myocyte gap junctions. Circ Res 1993;73:344-350.
4. Luke RA, Beyer EC, Hoyt RH, Saffitz JE. Quantitative analysis of intercellular connections by immunohistochemistry of the cardiac gap junction protein connexin43. Circ Res 1989;65:1450-1457.

5. Lerner DL, Yamada KA, Schuessler RB, Saffitz JE. Accelerated onset and increased incidence of ventricular arrhythmias induced by ischemia in Cx43-deficient mice. Circulation 2000;101:547-552.
6. Lammers WJEP, Schalij MJ, Kirchhof CJHJ, Allessie MA. Quantification of spatial inhomogeneity in conduction and initiation of reentrant atrial arrhythmias. Am J Physiol Heart Circ Physiol 1990;259:H1254-H1263.
7. Huang RY-C, Laing JG, Kanter EM, Berthoud VM, Bao M, Rohrs HW, Townsend RR, Yamada KA. Identification of CaMKII phosphorylation sites in connexin43 by high-resolution mass spectrometry. J Proteome Res 2011; 10:1098-1109.

Supplemental Figure Legends

Supplemental Figure S1. Immunoblot showing increasing protein amounts of 3 different Cx43 fusion protein preparations (A, B/C and D) and 2 different fractions from one preparation (B and C). There was a fair amount of variability from one preparation to another, which dictated that we run multiple quantitative immunoblots using multiple fusion protein preparations in order to be confident of the absolute protein determinations that are reported here. One ventricular sample from a wild-type (WT) mouse is shown in the 6^{th} lane to the right of the molecular weight markers.

Supplemental Figure S2. **A:** Representative immunoblot showing the specificity of a new anti-Cx45 antiserum. Affinity-purified antiserum recognized Cx45 (within the box) in HeLa cells transfected to overexpress Cx45 (lane 2), in ventricular myocardium from Cx45OEs (lane 4) more than in wild-type (WT, lane 5) myocardium, and in atria from Cx40 null/knock-in Cx45

(Cx45 KI, lane 6). The antiserum recognized the Cx45 CT fusion protein (fp) (asterisk, lane 8), but not Cx43 in HeLa cells transfected to overexpress Cx43 (lane 3) nor the Cx43 CT fp (lane 9). The membrane was reprobed with anti-GAPDH antibody to demonstrate equal loading of protein among cell and tissue homogenates, respectively. **B:** Immunoblot further demonstrating specificity of a new anti-Cx45 antiserum. Cx45 was recognized by the antiserum only in wild-type embryo homogenates (WT, lanes 1, 3, 5 and 7) and not in homogenates prepared from Cx45 knockout embryos (lanes 2, 4, 6 and 8). The membrane was stripped and reprobed with anti-GAPDH antibody to demonstrate equal loading of protein. **C:** Representative fluorescence images showing Cx45 immunoreactive signal in a ventricular myocardial tissue section from a wild-type (WT) mouse on the left, and stronger Cx45 signal in a section from a Cx45OE on the right. Bar = 50 μm. **D:** Representative fluorescence images showing atrial tissue sections stained with anti-Cx45 antiserum on the left and anti-Cx40 on the right. The top panels represent atrial tissue from Cx40 null/knockin Cx45 (Cx40 KO/Cx45 KI) hearts; the bottom panels represent atrial tissue from wild-type (WT) hearts. There is much stronger Cx45 immunoreactive signal in the Cx40 KO/Cx45 KI atrium (upper left) at intercellular junctions compared to trace signal in WT atrium (lower left). The panels on the right show that there is no Cx40 signal in the Cx40 KO/Cx45 KI atrium (upper right), but strong Cx40 signal at intercellular junctions in the WT atrium (lower right). Bar = 50 μm.

Supplemental Figure S3. Example of a quantitative immunoblot in which samples consisting of ventricular homogenates mixed with Cx45 fusion protein (Cx45 CT fp, ~20 kD) and thrombin-cleaved Cx43 fusion protein (Cx43 CT, ~15 kD, no GST) were loaded into each lane, except for the last lane which does not contain any tissue. The membrane was first probed with anti-Cx45

antibody (top), stripped and reprobed with anti-Cx43 antibody (bottom). Calculations of levels of Cx43 protein in ventricular myocardium using GST-Cx43 CT fusion protein compared with thrombin-cleaved Cx43 CT fusion protein were within the margin of error for each measurement.

Supplemental Figure S4. Representative QRS complexes from 2 control (Cre^{-};$Cx45^{fl/fl}$ and Cre^{+};$Cx45^{fl/+}$) and 2 cardiac-restricted Cx45-deficient mice (Cre^{+};$Cx45^{fl/fl}$). Lead I, II and III (top to bottom) were recorded from anesthetized mice in the supine position.

Supplemental Figure S5. Examples of isochronal maps obtained from optical action potentials recorded from the epicardial surface of a control heart (top panels) and a Cre^{+};$Cx45^{fl/fl}$ heart (bottom panels) perfused at 25ºC. Each color represents a 2 ms isochrone. The 16 x 16 photodiode array covered a 4 mm x 4 mm area with base at the top, apex toward the bottom, RV on the left, and LV on the right. Panels on the left were obtained after RV pacing at a cycle length of 180 ms; panels on the right were obtained after RV pacing at a cycle length of 130 ms. There were no remarkable differences in the pattern of activation or speed of propagation.

Supplemental Figure S6. CaMKII phosphorylation of Cx45 CT at S326 and T337. **A:** Extracted chromatogram of *m/z* 986.7701-986.7899. **B:** MS spectrum of *m/z* 986.7868 represents triply charged peptide ANIAQEQQYGSHEEHLPADLETLQR (one phosphorylation site). **C:** CID MS2 spectrum indicates peptide phosphorylated on S326. **D:** ETD MS2 spectrum indicates peptide phosphorylated on S326. **E:** Extracted chromatogram of *m/z* 986.7701-986.7899. **F:** MS spectrum of *m/z* 986.7861, represents triply charged peptide ANIAQEQQYGSHEEHLPADLETLQR (one phosphorylation site). **G:** CID MS2 spectrum

indicates peptide phosphorylated on T337. See Sup. Table S5 for complete list of theoretical (ProteinProspector) and observed fragment ions.

Supplemental Figure S7. CaMKII phosphorylation of Cx45 CT at S381, S382, S384, S385, S387. **A:** Extracted chromatogram of *m/z* 606.7288-606.7312. **B:** MS spectrum of *m/z* 606.7303 represents doubly charged peptide SSISSKSGDGK (two phosphorylation sites). **C:** ETD MS2 spectrum indicates peptide phosphorylated on S381 and S387. **D:** ETD MS2 spectrum indicates peptide phosphorylated on S382 and S387. **E:** ETD MS2 spectrum indicates peptide phosphorylated on S384 and S387. **F:** ETD MS2 spectrum indicates peptide phosphorylated on S385 and S387. See Sup. Table S6 for complete list of theoretical (ProteinProspector) and observed fragment ions.

Supplemental Figure S8. CaMKII phosphorylation of Cx45 CT at S381 and S382. **A:** Extracted chromatogram of *m/z* 581.7528-581.7532. **B:** MS spectrum of *m/z* 581.7520 represents doubly charged peptide SGSNKSSISSK (one phosphorylation site and one deamidated site). **C:** CID MS2 spectrum indicates peptide phosphorylated on S381. **D:** ETD MS2 spectrum indicates peptide phosphorylated on S381 and deamidated on N379. **E:** Extracted chromatogram of *m/z* 581.2608-581.2612. **F:** MS spectrum of *m/z* 581.2609 represents doubly charged peptide SGSNKSSISSK (one phosphorylation site). **G:** CID MS2 spectrum indicates peptide phosphorylated on S382. **H:** ETD MS2 spectrum indicates peptide phosphorylated on S382. See Sup. Table S7 for complete list of theoretical (ProteinProspector) and observed fragment ions.

Supplemental Figure S9. CaMKII phosphorylation of Cx45 CT at S384 and S387. **A:** Extracted chromatogram of *m/z* 378.1675-378.1680. **B:** MS spectrum of *m/z* 378.1679 represents triply charged peptide SSISSKSGDGK (one phosphorylation site). **C:** CID MS2 spectrum indicates peptide phosphorylated on S387. **D:** ETD MS2 spectrum indicates peptide phosphorylated on S387. **E:** CID MS2 spectrum indicates peptide phosphorylated on S384. See Sup. Table S8 for complete list of theoretical (ProteinProspector) and observed fragment ions.

Supplemental Figure S10. CaMKII phosphorylation of Cx45 CT at S393. **A:** Extracted chromatogram of *m/z* 565.7472-565.7528. **B:** MS spectrum of *m/z* 565.7474 represents doubly charged peptide SGDGKTSVWI (one phosphorylation site). **C:** CID MS2 spectrum indicates peptide phosphorylated on S393. **D:** ETD MS2 spectrum indicates peptide phosphorylated on S393. See Sup. Table S9 for complete list of theoretical (ProteinProspector) and observed fragment ions.

Supplemental Figure S11. CK1 phosphorylation of Cx45 CT at S326. **A:** Extracted chromatogram of *m/z* 1479.1734-1479.1764. **B:** MS spectrum of *m/z* 1479.1758 represents doubly charged peptide ANIAQEQQYGSHEEHLPADLETLQR (one phosphorylation site). **C:** CID MS2 spectrum indicates peptide phosphorylated on S326. See Sup. Table S10 for complete list of theoretical (ProteinProspector) and observed fragment ions.

Supplemental Figure S12. CK1 phosphorylation of Cx45 CT at S382. **A:** Extracted chromatogram of *m/z* 581.2602-581.2608. **B:** MS spectrum of *m/z* 581.2607 represents doubly charged peptide SGSNKSSISSK (one phosphorylation site). **C:** CID MS2 spectrum indicates

peptide phosphorylated on S382. See Sup. Table S11 for complete list of theoretical (ProteinProspector) and observed fragment ions.

Supplemental Figure S13. CK1 phosphorylation of Cx45 CT at S384 and S387. **A:** Extracted chromatogram of *m/z* 566.7474-566.7480. **B:** MS spectrum of *m/z* 566.7475 represents doubly charged peptide SSISSKSGDGK (one phosphorylation site). **C:** CID MS2 spectrum indicates peptide phosphorylated on S384. **D:** CID MS2 spectrum indicates peptide phosphorylated on S387. See Sup. Table S12 for complete list of theoretical (ProteinProspector) and observed fragment ions.

Supplemental Figure S14. CK1 phosphorylation of Cx45 CT at S393. **A:** Extracted chromatogram of *m/z* 565.2472-565.2528. **B:** MS spectrum of *m/z* 565.2495 represents doubly charged peptide SGDGKTSVWI (one phosphorylation site). **C:** CID MS2 spectrum indicates peptide phosphorylated on S393. See Sup. Table S13 for complete list of theoretical (ProteinProspector) and observed fragment ions.

Supplemental Tables

Supplemental Table S1. Ventricular activation times in cardiac Cx45-deficient ($Cre^{+};Cx45^{fl/fl}$) hearts.

	Spontaneous	RA paced	RV paced
FVB Controls	0.7 ± 1.2 (n = 8)	0.6 ± 0.7 (n = 6)	12.5 ± 2.7 (n = 8)
Cx45-deficient $Cre^{+};Cx45^{fl/fl}$	0.3 (n = 2)	1.0 (n = 2)	15.4 (n = 2)

Activation times (ms) are reported as mean ± SD and were measured between the RV endocardial apex and the LV epicardial lateral wall.
FVB controls included $Cre^{-};Cx45^{fl/fl}$ and $Cre^{+};Cx45^{fl/+}$ genotypes.

Supplemental Table S2. Conduction velocities and anisotropic ratios obtained from optical mapping of Cx45OE and wild-type hearts.

	RV S1	LVC S2, longitudinal	LVC S2, transverse	Anisotropic ratio
Wild-type (n = 6)	42.5 ±14.2 cm/s	40.0 ± 7.4 cm/s	21.0 ± 3.1 cm/s	1.9 ± 0.2
Cx45OE (n = 5)	37.3 ± 2.9 cm/s	38.6 ± 8.4 cm/s	20.4 ± 6.4 cm/s	2.0 ± 0.3

S1 stimulation at a cycle length (CL) of 180 ms was administered to the RV apex.
S2 stimulation at a coupling interval (CI) of 140 ms was administered at the center of the LV lateral free wall (LVC). Maximal (longitudinal) and minimal (transverse) orthogonal conduction velocities were measured from the elliptical spread of excitation from the S2 stimulus site and were used to calculate anisotropic ratios.

Supplemental Table S3. Ventricular activation times in Cx45OE hearts.

	Spontaneous	RA paced	RV paced
Wild-type	-0.1 ± 2.2 (n = 12)	0.3 ± 3.0 (n = 11)	11.0 ± 3.9 (n = 6)
Cx45OE	1.7 ± 1.9 (n = 6)	0.1 ± 0.9 (n = 5)	9.9 ± 2.3 (n = 5)

Activation times (ms) were measured between the RV endocardial apex and the LV epicardial lateral wall and are reported as mean ± SD.

Supplemental Table S4. Measurement of inhomogeneity of ventricular activation in Cx45OE hearts.

	Median	Range	Inhomogeneity Index
Wild-type (n = 5)	1.54 ± 0.10	2.77 ± 0.25	1.80 ± 0.17
Cx45OE (n = 3)	1.17 ± 0.76	2.58 ± 1.12	2.46 ± 0.57*

Values are given as mean ± SD. The range indicates the total range of maximal differences in activation times, excluding the lowest and highest 5% of values (P_5-P_{95}). The Inhomogeneity Index was calculated as (P_5-P_{95})/P_{50}, where P_{50} is the median.
*, p = 0.046

Suppl Table S5 for Fig S6

Cx45-37 #5713 @986.78 CID

S326 CID	b	b 2+	[b-NH3]	[b-NH3]2+	[b-H3PO4]	y	y 2+	[y-NH3]	[y-NH3]2+	[y-H3PO4]	[y-H3PO4]2+
A											
N	186.09		169.06			2886.31	1443.66	2869.28	1435.14	2788.33	1394.67
I	299.17 (299.22)		282.14			2772.26	1386.63	2755.24	1378.12	2674.29	1337.65 (1337.74)
A	370.21		353.18			2659.18	1330.09 (1330.77)	2642.15	1321.58	2561.20	1281.10 (1280.92)
Q	498.27 (498.10)		481.24			2588.14	1294.57	2571.11	1286.06	2490.16	1245.59 (1245.77)
E	627.31 (627.05)		610.28			2460.08	1230.55 (1230.27)	2443.06	1222.03 (1222.15)	2362.11	1181.56 (1181.66)
Q	755.37 (755.29)		738.34 (738.32)			2331.04	1166.02 (1166.66)	2314.01	1157.51 (1157.49)	2233.06	1117.04
Q	883.43 (883.51)		866.40 (866.71)			2202.98	1101.99 (1101.19)	2185.96	1093.48 (1093.50)	2105.00	1053.01
Y	1046.49 (1046.44)		1029.46			2074.92	1037.97	2057.90	1029.45 (1029.92)	1976.95	988.98
G	1103.51 (1103.62)		1086.49 (1086.44)			1911.86	956.43 (956.76)	1894.83	947.92 (947.64)	1813.88 (1813.95)	907.45 (907.38)
S	1270.51		1253.48		1172.53 (1172.30)	1854.84	927.92	1837.81	919.41 (919.25)	1756.86	878.93 (879.19)
H	1407.57 (1407.54)	704.29	1390.54	695.77	1309.59	1687.84	844.42 (844.47)	1670.81	835.91		
E	1536.61 (1536.75)	768.81	1519.58	760.30 (760.48)	1438.63 (1438.43)	1550.78 (1550.34)	775.89	1533.75	767.38		
E	1665.65	833.33	1648.63	824.82	1567.68 (1567.62)	1421.74	711.37 (711.42)	1404.71 (1404.89)	702.86 (702.41)		
H	1802.71 (1802.69)	901.86 (901.19)	1785.69	893.35 (893.08)	1704.74	1292.70 (1292.81)	646.85	1275.67 (1275.87)	638.34 (638.54)		
L	1915.80 (1915.27)	958.40 (958.41)	1898.77	949.89 (949.23)	1817.82	1155.64 (1155.70)	578.32	1138.61 (1138.67)	569.81		
P	2012.85	1006.93	1995.82	998.42	1914.87	1042.55	521.78 (521.91)	1025.53	513.27		
A	2083.89	1042.45 (1042.40)	2066.86	1033.93	1985.91	945.50	473.25	928.47	464.74		
D	2198.91	1099.96 (1099.99)	2181.89	1091.45 (1091.45)	2100.94	874.46 (874.45)	437.74	857.44 (857.51)	429.22		
L	2312.00	1156.50 (1156.52)	2294.97	1147.99 (1147.79)	2214.02	759.44 (759.47)	380.22	742.41	371.71		
E	2441.04	1221.02 (1221.40)	2424.01	1212.51 (1212.66)	2343.06	646.35 (646.75)	323.68	629.33	315.17		
T	2542.09	1271.55 (1271.84)	2525.06	1263.03	2444.11	517.31 (517.01)	259.16	500.28	250.65		
L	2655.17	1328.09	2638.15	1319.58	2557.20	416.26	208.63	399.24	200.12		
Q	2783.23	1392.12 (1392.11)	2766.20	1383.61	2685.25	303.18	152.09	286.15	143.58		
R						175.12	88.06	158.09	79.55		

[M-H3PO4+3H]3+	954.08
[M-H3PO4-NH3+3H]3+	948.51

Yellow:	Out of spectrum mass range
Red:	Relative intensity >0.5
Theoretical m/z (Observed m/z)	

Cx45-37 #4506-6854 @986.78 ETD

S326 ETD	c	[c+1]	z	z 2+	[z+1]	[z+1]2+	[z+2]
A							
N	203.11	204.12	2870.29	1435.65 (1435.75)	2871.29	1436.15	2872.30
I	316.20	317.20	2756.24	1378.63 (1378.75)	2757.25	1379.13 (1379.53)	2758.25
A	387.24	388.24	2643.16	1322.08	2644.17	1322.59 (1322.23)	2645.17
Q	515.29	516.30 (516.86)	2572.12	1286.56 (1286.56)	2573.13	1287.07	2574.13
E	644.34 (644.34)	645.34 (645.25)	2444.06	1222.54	2445.07	1223.04 (1222.96)	2446.08
Q	772.39 (772.35)	773.4 (773.43)	2315.02	1158.01	2316.03	1158.52	2317.03
Q	900.45 (900.34)	901.46 (901.59)	2186.96	1093.99	2187.97	1094.49	2188.97
Y	1063.52 (1063.41)	1064.52 (1064.04)	2058.90	1029.96	2059.91	1030.46	2060.92
G	1120.54 (1120.34)	1121.54 (1121.39)	1895.84	948.42	1896.85 (1896.63)	948.93	1897.85 (1897.76)
S	1287.54 (1287.44)	1288.54 (1288.46)	1838.82 (1838.65)	919.91	1839.83 (1839.77)	920.42	1840.83 (1840.74)
H	1424.60 (1424.48)	1425.60	1671.82 (1671.97)	836.41	1672.83 (1672.77)	836.92	1673.83 (1673.83)
E	1553.64 (1553.40)	1554.64 (1554.42)	1534.76 (1534.43)	767.88	1535.77 (1535.61)	768.39	1536.77 (1536.72)
E	1682.68 (1682.52)	1683.68 (1683.44)	1405.72	703.36	1406.73 (1406.66)	703.87	1407.73 (1407.68)
H	1819.74 (1819.74)	1820.74 (1820.64)	1276.68 (1276.37)	638.84	1277.68 (1277.57)	639.35	1278.69 (1278.61)
L			1139.62 (1139.35)		1140.63 (1140.47)		1141.63 (1141.62)
P	2029.88	2030.88					
A	2100.91	2101.92	929.48 (929.29)		930.49 (930.44)		931.49 (931.52)
D	2215.94	2216.94	858.44 (858.78)		859.45 (859.33)		860.45 (860.53)
L	2329.02	2330.03	743.42 (743.45)		744.43 (744.48)		745.43 (745.53)
E	2458.07	2459.07	630.33 (630.33)		631.34 (631.34)		632.34 (632.53)
T	2559.11	2560.12	501.29 (501.53)		502.30 (502.36)		503.30 (503.36)
L	2672.20	2673.20	400.24 (400.35)		401.25 (401.30)		402.25 (402.24)
Q	2800.26	2801.26	287.16 (287.05)		288.17 (288.23)		289.17 (289.41)
R			159.10		160.11		161.11

[M+3H]3+	987.14
[M+2H]2+	1479.71

Yellow:	Out of spectrum mass range
Red:	Relative intensity >0.1
Theoretical m/z (Observed m/z)	

Cx45-29-10 #2830-2838 @986.78 CID

T337 CID	b	b 2+	[b-NH3]	[b-H2O]	[b-H3PO4]2+	y	y 2+	[y-NH3]	[y-NH3]2+	[y-H2O]	[y-H2O]2+	[y-H3PO4]	[y-H3PO4]2+
A													
N	186.09		169.06			2886.31	1443.66	2869.28	1435.14	2868.29	1434.65	2788.33	1394.67
I	299.17 (299.09)		282.14			2772.26	1386.63 (1386.91)	2755.24	1378.12	2754.25	1377.63	2674.29	1337.65 (1337.55)
A	370.21 (370.00)		353.18 (353.09)			2659.18	1330.09 (1330.36)	2642.15	1321.58 (1321.36)	2641.17	1321.09	2561.20	1281.10 (1281.45)
Q	498.27 (498.27)		481.24 (481.18)			2588.14	1294.57	2571.11	1286.06 (1286.27)	2570.13	1285.57	2490.16	1245.59 (1245.91)
E	627.31 (627.18)		610.28 (610.36)	609.30 (609.27)		2460.08	1230.55 (1230.82)	2443.06	1222.03	2442.07	1221.54 (1221.82)	2362.11	1181.56
Q	755.37 (755.36)		738.34	737.36		2331.04	1166.02	2314.01	1157.51 (1157.91)	2313.03	1157.02 (1157.36)	2233.06	1117.04 (1117.00)
Q	883.43		866.40	865.42		2202.98	1101.99	2185.96	1093.48 (1093.45)	2184.97	1092.99	2105.00	1053.01
Y	1046.49		1029.46	1028.48		2074.92	1037.97	2057.90	1029.45 (1029.27)	2056.91	1028.96	1976.95	988.98
G	1103.51		1086.49	1085.50		1911.86	956.43	1894.83	947.92	1893.85	947.43	1813.88 (1813.73)	907.45 (907.45)
S	1190.54		1173.52	1172.53 (1172.91)		1854.84	927.92	1837.81 (1837.45)	919.41	1836.83 (1836.55)	918.92	1756.86 (1756.82)	878.93
H	1327.60	664.30	1310.58	1309.59		1767.81	884.41	1750.78 (1750.55)	875.89	1749.80 (1749.73)	875.40	1669.83	835.42 (835.91)
E	1456.65 (1456.36)	728.83	1439.62	1438.63		1630.75	815.88	1613.72	807.36	1612.74	806.87	1532.77	766.89
E	1585.69 (1585.36)	793.35	1568.66	1567.68		1501.70	751.36	1484.68	742.84	1483.69	742.35 (742.27)	1403.73	702.37 (702.36)
H	1722.75 (1722.18)	861.88 (861.91)	1705.72	1704.74		1372.66	686.83	1355.64	678.32	1354.65	677.83 (677.36)	1274.69	637.85 (637.82)
L	1835.83 (1835.45)	918.42 (918.36)	1818.80	1817.82		1235.60	618.31 (618.36)	1218.58	609.79	1217.59	609.30 (609.27)	1137.63 (1137.55)	569.32
P	1932.88	966.95	1915.86	1914.87		1122.52 (1122.36)	561.76 (561.73)	1105.49	553.25	1104.51	552.76	1024.54 (1024.45)	512.77 (512.64)
A	2003.92	1002.46	1986.89	1985.91		1025.47 (1025.45)	513.24 (513.36)	1008.44	504.72	1007.46	504.23	927.49	464.25 (464.09)
D	2118.95	1059.98	2101.92	2100.94		954.43	477.72	937.40	469.21	936.42	468.71	856.45	428.73
L	2232.03	1116.52	2215.01	2214.02		839.40 (839.27)	420.20	822.38	411.69	821.39	411.20	741.43 (741.45)	371.22
E	2361.07	1181.04 (1181.45)	2344.05	2343.06		726.32	363.66	709.29	355.15	708.31	354.66	628.34 (628.27)	314.67
T	2542.09	1271.55	2525.06	2524.08	1222.56 (1222.45)	597.28 (597.27)	299.14 (299.09)	580.25	290.63			499.30 (499.36)	250.15
L	2655.17	1328.09	2638.15	2637.16	1279.10	416.26 (416.36)	208.63	399.24	200.12				
Q	2783.23	1392.12 (1392.36)	2766.20	2765.22	1343.13 (1343.36)	303.18 (303.27)	152.09	286.15	143.58				
R						175.12	88.06	158.09	79.55				

[M-H3PO4+3H]3+	954.09
[M-H3PO4-NH3+3H]3+	948.09

Yellow:	Out of spectrum mass range
Red:	Relative intensity >0.2
Theoretical m/z (Observed m/z)	

Suppl Table S6 for Fig S7

Cx45-37 #1680 @606.73 ETD

S381, S387	c	[c+1]	z	[z+1]	[z+2]
S					
S	272.06	273.07	1029.44 (1029.32)	1030.45 (1030.45)	1031.45 (1031.37)
I	385.15	386.15	942.41 (942.28)	943.41 (943.09)	944.42 (944.51)
S	472.18	473.18	829.32 (829.04)	830.33 (830.57)	831.33 (831.33)
S	559.21	560.22	742.29 (742.28)	743.30 (743.22)	744.30 (744.31)
K	687.31 (687.15)	688.31 (688.26)	655.26 (655.20)	656.27 (656.63)	657.27
S	854.31 (854.27)	855.31	527.16	528.17	529.17
G	911.33 (911.23)	912.33 (912.42)	360.16	361.17	362.18
D	1026.35 (1026.31)	1027.36	303.14	304.15	305.15
G	1083.38 (1083.29)	1084.38 (1084.31)	188.12	189.12	190.13
K			131.09	132.10	133.11

[M+2H]2+	606.67

Yellow:	Out of spectrum mass range
Red:	Relative intensity >0.2
Theoretical m/z (Observed m/z)	

Cx45-37 #1745 @606.73 ETD

S382, S387	c	[c+1]	z	[z+1]
S				
S	272.06	273.07	1109.40 (1109.20)	1110.41 (1110.30)
I	385.15	386.15	942.41 (942.55)	943.41 (943.58)
S	472.18	473.18	829.32 (829.34)	830.33
S	559.21	560.22	742.29 (742.25)	743.30
K	687.31	688.31	655.26 (655.26)	656.27 (656.21)
S	854.31 (854.25)	855.31 (855.14)	527.16	528.17
G	911.33 (911.22)	912.33 (912.56)	360.16	361.17
D	1026.35 (1026.13)	1027.36	303.14	304.15
G	1083.38 (1083.24)	1084.38 (1084.36)	188.12	189.12
K			131.09	132.10

[M+2H]2+	606.63

Yellow:	Out of spectrum mass range
Red:	Relative intensity >0.2
Theoretical m/z (Observed m/z)	

Cx45-37 #1828 @606.73 ETD

S384, S387	c	[c+1]	z	[z+1]
S				
S	192.10	193.10	1109.40 (1109.16)	1110.41 (1110.05)
I	305.18	306.19	1022.37	1023.38 (1023.48)
S	472.18	473.18	909.29 (909.26)	910.30 (910.19)
S	559.21	560.22	742.29 (742.66)	743.30 (743.29)
K	687.31 (687.18)	688.31	655.26 (655.74)	656.27 (656.84)
S	854.31 (854.33)	855.31 (855.30)	527.16	528.17
G	911.33 (911.20)	912.33 (911.98)	360.16	361.17
D	1026.35 (1026.47)	1027.36	303.14	304.15
G	1083.38 (1083.28)	1084.38 (1084.35)	188.12	189.12
K			131.09	132.10

[M+2H]2+	606.77

Yellow:	Out of spectrum mass range
Red:	Relative intensity >0.2
Theoretical m/z (Observed m/z)	

Cx45-37 #1808 @606.73 ETD

S385, S387	c	[c+1]	z	[z+1]
S				
S	192.10	193.10	1109.40 (1109.29)	1110.41 (1110.21)
I	305.18	306.19	1022.37 (1022.34)	1023.38 (1023.46)
S	392.21	393.22	909.29 (909.85)	910.30 (910.95)
S	559.21	560.22	822.26 (822.84)	823.26 (823.83)
K	687.31 (687.42)	688.31 (688.09)	655.26 (655.49)	656.27 (656.24)
S	854.31 (854.12)	855.31 (855.56)	527.16	528.17 (528.47)
G	911.33 (911.98)	912.33 (912.66)	360.16	361.17
D	1026.35 (1026.39)	1027.36 (1027.44)	303.14	304.15
G	1083.38 (1083.29)	1084.38 (1084.24)	188.12	189.12
K			131.09	132.10

[M+2H]2+	606.93

Yellow:	Out of spectrum mass range
Red:	Relative intensity >0.2
Theoretical m/z (Observed m/z)	

Suppl Table S7 for Fig S8

Cx45-37 #1622 @581.75 CID

S381 CID	b	b 2+	[b-NH3]	[b-NH3]2+	[b-H2O]	[b-H2O]2+	[b-H3PO4]	[b-H3PO4]2+	y	y 2+	[y-NH3]	[y-NH3]2+	[y-H2O]	[y-H2O]2+	[y-H3PO4]	[y-H3PO4]2+
S																
G	145.06				127.05				1075.47	538.24 (538.24)	1058.44	529.72 (529.86)	1057.46	529.23 (529.06)	977.49	489.25 (489.44)
S	232.09 (232.30)				214.08 (214.24)				1018.45 (1018.51)	509.73 (509.45)	1001.42	501.21	1000.43	500.72	920.47 (920.73)	460.74 (460.71)
N (Deamidated)	347.12		330.09 (330.20)		329.11 (329.49)				931.41 (931.47)	466.21 (466.31)	914.39	457.70	913.40	457.21	833.44	417.22
K	475.21 (475.24)	238.11 (238.31)	458.19 (458.21)	229.60	457.20 (457.31)	229.11			816.39 (816.47)	408.70 (408.87)	799.36	400.18	798.38 (798.47)	399.69	718.41 (718.30)	359.71 (359.87)
S	642.21	321.61 (321.32)	625.19	313.10 (313.18)	624.20	312.60	544.24 (544.31)	272.62	688.29 (688.40)	344.65	671.26	336.14 (336.56)	670.28	335.64	590.31 (590.31)	295.66 (295.05)
S	729.25	365.13	712.22	356.61	711.23	356.12	631.27 (631.26)	316.14	521.29	261.15	504.27 (504.17)	252.64	503.28 (503.33)	252.14		
I	842.33 (842.39)	421.67	825.30 (825.17)	413.15 (413.83)	824.32	412.66 (412.76)	744.35 (744.29)	372.68	434.26 (434.48)	217.63	417.23 (417.14)	209.12 (209.07)	416.25	208.63		
S	929.36	465.18	912.33	456.67	911.35	456.18 (456.32)	831.38	416.20	321.18	161.09	304.15	152.58	303.17	152.09		
S	1016.39	508.70 (508.24)	999.37 (999.87)	500.19 (500.86)	998.38	499.70 (499.84)	918.42 (918.46)	459.71 (459.71)	234.14 (234.29)	117.58	217.12	109.06	216.13 (216.10)	108.57		
K									147.11	74.06	130.09	65.55				

[M-H3PO4+2H]2+	532.46
[M-H3PO4-H2O+2H]2+	523.51

Yellow:	Out of spectrum mass range
Red:	Relative intensity >0.2
Theoretical m/z (Observed m/z)	

Cx45-37 #1521-3969 @581.75 ETD

S381 ETD	c	[c+1]	z	[z+1]
S				
G	162.09	163.09	1059.45 (1059.33)	1060.46 (1060.29)
S	249.12	250.12	1002.43 (1002.26)	1003.43 (1003.34)
N (Deamidated)	364.15	365.15	915.39 (915.24)	916.40 (916.33)
K	492.24 (492.33)	493.24	800.37 (800.26)	801.38 (801.35)
S	659.24	660.24	672.27 (672.62)	673.28 (673.28)
S	746.27 (746.34)	747.28 (747.21)	505.27	506.28 (506.31)
I	859.36 (859.39)	860.36 (860.30)	418.24	419.25 (419.56)
S	946.39 (946.37)	947.39 (947.42)	305.16	306.17
S	1033.42 (1033.39)	1034.42 (1034.42)	218.13	219.13
K			131.09	132.10

[M+2H]2+		581.49

Yellow:	Out of spectrum mass range
Red:	Relative intensity >0.1
Theoretical m/z (Observed m/z)	

Cx45-37 #1614 @581.26 CID

S382 CID	b	b 2+	[b-NH3]	[b-H2O]	[b-H3PO4]	[b-H3PO4]2+	y	y 2+	[y-NH3]	[y-NH3]2+	[y-H2O]	[y-H2O]2+	[y-H3PO4]	[y-H3PO4]2+
S														
G	145.06			127.05			1074.48	537.75 (537.05)	1057.46	529.23 (529.30)	1056.47	528.74 (528.45)	976.51	488.76 (488.81)
S	232.09 (232.13)			214.08			1017.46	509.23	1000.43	500.72 (500.87)	999.45	500.23	919.48	460.25 (460.40)
N	346.14 (346.21)		329.11 (329.34)	328.13 (328.19)			930.43 (930.20)	465.72 (465.89)	913.40 (913.47)	457.21	912.42	456.71	832.45	416.73
K	474.23 (474.36)	237.62	457.20 (457.23)	456.22 (455.99)			816.39 (816.57)	408.70 (408.43)	799.36	400.18	798.38 (798.59)	399.69 (399.36)	718.41 (718.50)	359.71 (359.83)
S	561.26	281.14	544.24 (544.46)	543.25 (543.48)			688.29 (688.28)	344.65	671.26	336.14	670.28	335.64	590.31 (590.33)	295.66 (295.26)
S	728.26	364.63	711.23	710.25	630.28 (630.33)	315.65	601.26 (601.17)	301.13 (301.96)	584.23	292.62	583.25	292.13	503.28 (503.28)	252.14
I	841.35	421.18 (421.78)	824.32 (824.27)	823.33 (823.07)	743.37 (743.43)	372.19 (372.19)	434.26 (434.31)	217.63	417.23 (417.40)	209.12 (209.35)	416.25 (416.57)	208.63		
S	928.38 (928.24)	464.69	911.35 (911.42)	910.37 (910.46)	830.40	415.70	321.18 (321.24)	161.09	304.15	152.58	303.17 (303.18)	152.09		
S	1015.41 (1015.37)	508.21 (508.86)	998.38	997.40	917.43 (917.48)	459.22	234.14 (234.24)	117.58	217.12	109.06	216.13	108.57		
K							147.11	74.06	130.09	65.55				

[M-H3PO4+2H]2+	532.24
[M-H3PO4-H2O+2H]2+	523.5

Yellow:	Out of spectrum mass range
Red:	Relative intensity >0.2

Cx45-37 #1708 @581.26 ETD

S382 ETD	c	[c+1]	z	[z+1]	[z+2]
S					
G	162.09	163.09	1058.46 (1058.85)	1059.47 (1059.59)	1060.48 (1060.43)
S	249.12	250.12	1001.44 (1001.16)	1002.45 (1002.36)	1003.45 (1003.41)
N	363.16	364.17	914.41 (914.31)	915.42 (915.35)	916.42 (916.41)
K	491.26 (491.18)	492.26	800.37 (800.32)	801.38 (801.34)	802.38 (802.26)
S	578.29 (578.37)	579.29 (579.81)	672.27	673.28 (673.51)	674.28 (674.31)
S	745.29 (745.34)	746.29 (746.48)	585.24 (585.40)	586.25 (586.25)	587.25
I	858.37 (858.31)	859.38 (859.15)	418.24	419.25 (419.49)	420.25
S	945.40 (945.35)	946.41 (946.46)	305.16	306.17	307.17
S	1032.44 (1032.32)	1033.44 (1033.38)	218.13	219.13	220.14
K			131.09	132.10	133.11

[M+2H]2+		581.9

Yellow:	Out of spectrum mass range
Red:	Relative intensity >0.2
Theoretical m/z (Observed m/z)	

Suppl Table S8 for Fig S9

Cx45-37 #1579 @378.17 CID

S387 CID	b	b 2+	[b-NH3]	[b-H2O]	[b-H2O]2+	[b-H3PO4]2+	y	y 2+	[y-NH3]2+	[y-H2O]2+	[y-H3PO4]	[y-H3PO4]2+
S												
S	175.07			157.06 (157.34)			1045.46	523.23 (523.42)	514.72 (514.45)	514.23	947.48	474.24 (474.19)
I	288.16			270.14 (270.22)			958.42	479.72 (479.66)	471.20 (471.41)	470.71 (470.60)	860.45	430.73 (430.70)
S	375.19			357.18			845.34	423.17 (423.36)	414.66 (414.99)	414.17 (414.37)	747.36 (747.43)	374.19 (374.63)
S	462.22 (462.77)			444.21			758.31 (758.16)	379.66 (379.88)	371.14	370.65	660.33 (660.64)	330.67 (330.73)
K	590.31 (590.11)	295.66	573.29	572.30 (572.66)	286.66 (286.84)		671.28	336.14 (336.06)	327.63	327.14	573.30 (573.35)	287.15
S	757.31	379.16 (378.90)	740.29 (740.19)	739.30	370.15	330.17	543.18 (543.29)	272.09	263.58	263.09	445.20 (445.32)	223.11 (223.28)
G	814.33	407.67 (407.49)	797.31	796.32	398.67 (398.43)	358.68	376.18	188.60	180.08	179.59		
D	929.36	465.18 (465.22)	912.33	911.35	456.18 (456.19)	416.20 (416.20)	319.16 (319.68)	160.08	151.57	151.08		
G	986.38	493.70	969.36	968.37	484.69	444.71	204.13 (204.22)	102.57	94.06			
K							147.11 (147.23)	74.06	65.55			

[M-H3PO4+3H]3+	345.67

Yellow:	Out of spectrum mass range
Red:	Relative intensity >0.2
Theoretical m/z (Observed m/z)	

Cx45-37 #1563 @378.17 ETD

S387 ETD	c	c 2+	[c+1]	[c+1]2+	z	z 2+	[z+1]
S							
S	192.10		193.10		1029.44 (1029.05)	515.22 (515.53)	1030.45 (1030.33)
I	305.18 (305.17)		306.19 (306.18)		942.41 (942.35)	471.71 (471.57)	943.41 (943.82)
S	392.21 (392.18)		393.22 (393.08)		829.32 (829.17)	415.16 (414.98)	830.33 (830.15)
S	479.25 (479.20)		480.25 (480.17)		742.29 (742.08)	371.65	743.30 (743.51)
K	607.34 (607.54)	304.17 (304.33)	608.34 (608.44)	304.68	655.26 (655.25)	328.13	656.27 (656.31)
S	774.34 (774.27)	387.67	775.34 (775.39)	388.18	527.16 (527.18)		528.17 (528.05)
G	831.36 (831.34)	416.18 (416.01)	832.36 (832.46)	416.69 (416.88)	360.16 (360.02)		361.17 (361.22)
D	946.39 (946.33)	473.70	947.39 (947.47)	474.20	303.14 (303.10)		304.15
G	1003.41 (1003.47)	502.21	1004.41 (1004.49)	502.71	188.12		189.12
K					131.09		132.10

[M+3H]3+	378.29

Yellow:	Out of spectrum mass range
Red:	Relative intensity >0.5
Theoretical m/z (Observed m/z)	

Cx45-37 #1721 @378.17 CID

S384 CID	b	b 2+	[b-NH3]2+	[b-H3PO4]	[b-H3PO4]2+	y	y 2+	[y-NH3]	[y-NH3]2+	[y-H2O]	[y-H3PO4]	[y-H3PO4]2+
S												
S	175.07 (175.20)					1045.46	523.23 (523.29)	1028.43	514.72 (514.69)	1027.45	947.48	474.24 (474.26)
I	288.16 (288.26)					958.42	479.72 (479.69)	941.40	471.20 (471.56)	940.41	860.45	430.73 (430.96)
S	455.15			357.18		845.34	423.17 (423.15)	828.31	414.66 (414.26)	827.33	747.36 (747.61)	374.19
S	542.19			444.21 (444.80)		678.34	339.67 (339.59)	661.32	331.16	660.33 (660.33)		
K	670.28	335.64 (335.02)	327.13 (327.63)	572.30	286.66	591.31	296.16	574.28 (574.46)	287.65 (287.57)	573.30 (573.36)		
S	757.31	379.16 (379.12)	370.65	659.34	330.17 (330.52)	463.21 (463.19)	232.11	446.19	223.60 (223.27)	445.20 (445.53)		
G	814.33	407.67 (407.23)	399.16 (399.28)	716.36 (716.51)	358.68	376.18	188.60	359.16	180.08	358.17		
D	929.36	465.18 (465.46)	456.67 (456.34)	831.38	416.20 (416.24)	319.16	160.08	302.13 (302.91)	151.57 (151.12)	301.15		
G	986.38	493.70	485.18	888.41	444.71	204.13 (204.21)	102.57	187.11 (187.35)	94.06			
K						147.11 (147.14)	74.06	130.09 (130.06)	65.55			

[M-H3PO4+3H]3+	345.67

Yellow:	Out of spectrum mass range
Red:	Relative intensity >0.5
Theoretical m/z (Observed m/z)	

Suppl Table S9 for Fig S10

Cx45-37 #4729 @565.75 CID

S393 CID	b	b 2+	[b-NH3]	[b-H2O]	[b-H3PO4]	[b-H3PO4]2+	y	y 2+	[y-NH3]2+	[y-H2O]2+	[y-H3PO4]	[y-H3PO4]2+
S												
G	145.06			127.05			1042.46 (1042.35)	521.73 (521.76)	513.22	512.73 (512.94)	944.48	472.75 (472.81)
D	260.09 (259.97)			242.08			985.44 (985.35)	493.22 (493.28)	484.71 (484.43)	484.22	887.46 (887.42)	444.23 (444.30)
G	317.11 (317.13)			299.10			870.41 (870.30)	435.71 (435.27)	427.20	426.70	772.44 (772.30)	386.72
K	445.20 (445.36)	223.11	428.18 (428.39)	427.19 (427.46)			813.39 (813.25)	407.20 (407.40)	398.69 (398.88)	398.19 (398.01)	715.41 (715.37)	358.21 (358.30)
T	546.25	273.63 (273.37)	529.23 (529.74)	528.24 (528.46)			685.30 (685.17)				587.32 (587.36)	
S	713.25	357.13 (357.15)	696.22 (696.30)	695.24	615.27 (615.24)	308.14	584.25 (584.17)				486.27 (486.32)	
V	812.32 (812.24)	406.66 (406.49)	795.29 (795.34)	794.31 (794.24)	714.34 (714.22)	357.67	417.25 (417.26)					
W	998.40 (998.27)	499.70 (499.64)	981.37 (981.34)	980.39 (980.24)	900.42 (900.35)	450.71 (450.93)	318.18 (318.22)					
I							132.10					

[M-H3PO4+2H]2+	516.47
[M-H3PO4-H2O+2H]2+	507.44

Yellow:	Out of spectrum mass range
Red:	Relative intensity >0.2
Theoretical m/z (Observed m/z)	

Cx45-37 #4697 @565.75 ETD

S393 ETD	c	[c+1]	z	[z+1]
S				
G	162.09	163.09	1026.44 (1026.17)	1027.45 (1027.21)
D	277.11	278.12	969.42 (969.12)	970.43 (970.22)
G	334.14	335.14	854.39 (854.19)	855.40 (855.33)
K	462.23 (462.25)	463.23 (463.40)	797.37 (797.22)	798.38 (798.26)
T	563.28 (563.41)	564.28 (564.90)		
S	730.28 (730.28)	731.28 (731.37)		
V	829.35 (829.39)	830.35 (830.37)		
W	1015.42 (1015.35)	1016.43 (1016.38)		
I				

[M+2H]2+	565.51

Yellow:	Out of spectrum mass range
Red:	Relative intensity >0.1
Theoretical m/z (Observed m/z)	

Suppl Table S10 for Fig S11

Cx45-29-11 #2670 @1479.17 CID

S326 CID	b	b 2+	[b-NH3]	[b-H3PO4]	y	y 2+	[y-H2O]	[y-H3PO4]	[y-H3PO4]2+
A									
N	186.09		169.06		2886.31	1443.66	2868.29	2788.33	1394.67
I	299.17		282.14		2772.26	1386.63 (1386.36)	2754.25	2674.29	1337.65 (1337.45)
A	370.21		353.18		2659.18	1330.09 (1330.00)	2641.17	2561.20	1281.10 (1281.18)
Q	498.27		481.24		2588.14	1294.57	2570.13	2490.16	1245.59 (1245.45)
E	627.31		610.28		2460.08	1230.55	2442.07	2362.11	1181.56 (1181.45)
Q	755.37		738.34		2331.04	1166.02	2313.03	2233.06	1117.04 (1116.91)
Q	883.43 (883.09)		866.40 (866.27)		2202.98	1101.99	2184.97	2105.00	1053.01
Y	1046.49 (1046.36)		1029.46 (1029.18)		2074.92	1037.97	2056.91	1976.95 (1976.64)	988.98 (988.82)
G	1103.51 (1103.09)		1086.49		1911.86 (1911.55)	956.43	1893.85	1813.88 (1813.27)	907.45
S	1407.57		1253.48	1172.53 (1172.27)	1854.84 (1854.55)	927.92 (927.73)	1836.83	1756.86 (1756.36)	878.93
H	1536.61	704.29	1390.54	1309.59 (1309.18)	1687.84	844.42	1669.83 (1669.36)		
E	1665.65 (1665.36)	768.81	1519.58	1438.63 (1438.18)	1550.78 (1550.45)	775.89	1532.77 (1532.55)		
E	1687.64 (1687.64)	833.33	1648.63	1567.68 (1567.55)	1421.74	711.37	1403.73		
H	1802.71 (1802.18)	901.86	1785.69	1704.74 (1704.27)	1292.70 (1292.36)	646.85	1274.69 (1274.45)		
L	1915.80 (1915.55)	958.40 (958.27)	1898.77	1817.82 (1817.55)	1155.64 (1155.36)	578.32	1137.63 (1137.64)		
P	2012.85	1006.93 (1006.36)	1995.82	1914.87	1042.55	521.78	1024.54 (1024.55)		
A	2083.89	1042.45 (1042.36)	2066.86	1985.91 (1985.36)	945.50 (945.27)	473.25	927.49		
D	2198.91	1099.96	2181.89	2100.94	874.46 (874.36)	437.74	856.45 (856.36)		
L	2312.00	1156.50	2294.97	2214.02	759.44 (759.36)	380.22	741.43 (741.36)		
E	2441.04	1221.02	2424.01	2343.06	646.35 (646.27)	323.68	628.34 (628.36)		
T	2542.09	1271.55	2525.06	2444.11	517.31 (517.18)	259.16	499.30 (499.36)		
L	2655.17	1328.09 (1328.36)	2638.15	2557.20	416.26	208.63			
Q	2783.23	1392.12	2766.20	2685.25	303.18	152.09			
R					175.12	88.06			

[M-H3PO4+2H]2+	1430
[M-H3PO4-H2O+2H]2+	1421

Yellow:	Out of spectrum mass range
Red:	Relative intensity >0.1
Theoretical m/z (Observed m/z)	

Suppl Table S11 for Fig S12

Cx45-29-11 #310-478 @581.26 CID

S382 CID	b	[b-NH3]	[b-H2O]	[b-H3PO4]	y	y 2+	[y-H2O]	[y-H3PO4]	[y-H3PO4]2+
S									
G	145.06		127.05		1074.48 (1074.45)	537.75	1056.47	976.51	488.76
S	232.09 (232.09)		214.08 (214.09)		1017.46	509.23 (509.27)	999.45	919.48	460.25 (460.36)
N	346.14 (346.09)	329.11	328.13 (328.18)		930.43 (930.27)	465.72 (465.82)	912.42	832.45 (832.36)	416.73 (416.73)
K	474.23 (474.27)	457.20 (457.27)	456.22 (456.18)		816.39 (816.27)	408.70	798.38 (798.27)	718.41 (718.27)	359.71
S	561.26	544.24	543.25 (543.27)		688.29 (688.18)	344.65	670.28 (670.18)	590.31 (590.27)	295.66 (295.18)
S	728.26 (728.18)	711.23	710.25	630.28 (630.27)	601.26 (601.18)	301.13	583.25	503.28 (503.27)	252.14
I	841.35 (841.18)	824.32 (824.18)	823.33 (823.27)	743.37 (743.27)	434.26 (434.36)	217.63	416.25		
S	928.38 (928.18)	911.35 (911.18)	910.37 (910.18)	830.40 (830.36)	321.18 (321.18)	161.09	303.17 (303.18)		
S	1015.41 (1015.18)	998.38	997.40 (997.27)	917.43 (917.36)	234.14 (234.18)	117.58	216.13 (216.09)		
K					147.11	74.06			

[M-H3PO4+2H]2+	532.36
[M-H3PO4-H2O+2H]2+	523.27

Yellow:	Out of spectrum mass range
Red:	Relative intensity >0.1
Theoretical m/z (Observed m/z)	

Suppl Table S12 for Fig S13

Cx45-29-11 #324 @566.75 CID

S384 CID	b	[b-NH3]	[b-NH3] 2+	[b-H2O]	[b-H3PO4]	y	[y-NH3]	[y-H2O]	[y-H3PO4]	[y-H3PO4]2+
S										
S	175.07 (175.00)			157.06		1045.46	1028.43	1027.45	947.48	474.24 (474.27)
I	288.16 (288.09)			270.14 (270.09)		958.42 (958.09)	941.40	940.41	860.45 (860.36)	430.73 (430.73)
S	455.15			437.14	357.18 (357.18)	845.34 (845.18)	828.31	827.33 (827.27)	747.36 (747.36)	374.19 (374.18)
S	542.19			524.18	444.21 (444.27)	678.34	661.32 (661.27)	660.33 (660.27)		
K	670.28	653.25 (653.27)	327.13	652.27	572.30 (572.18)	591.31 (591.27)	574.28	573.30		
S	757.31	740.29 (740.36)	370.65	739.30	659.34 (659.27)	463.21	446.19 (446.27)	445.20 (445.27)		
G	814.33	797.31	399.16 (399.18)	796.32 (796.27)	716.36 (716.36)	376.18 (376.18)	359.16	358.17		
D	929.36 (929.18)	912.33	456.67	911.35 (911.27)	831.38 (831.36)	319.16 (319.18)	302.13	301.15		
G	986.38 (986.27)	969.36	485.18	968.37 (968.45)	888.41 (888.45)	204.13 (204.09)	187.11			
K						147.11	130.09			

[M-H3PO4+2H]2+	517.82
[M-H3PO4-H2O+2H]2+	508.82

Yellow:	Out of spectrum mass range
Red:	Relative intensity >0.1
Theoretical m/z (Observed m/z)	

Cx45-29-11 #322 @566.75 CID

S387 CID	b	[b-NH3]	[b-H3PO4]	y	y 2+	[y-NH3]	[y-H2O]	[y-H3PO4]	[y-H3PO4]2+
S									
S	175.07 (175.00)			1045.46	523.23	1028.43 (1028.36)	1027.45	947.48	474.24 (474.18)
I	288.16 (288.00)			958.42 (958.27)	479.72 (479.82)	941.40	940.41	860.45 (860.36)	430.73 (430.82)
S	375.19			845.34 (845.27)	423.17 (423.18)	828.31	827.33 (827.18)	747.36 (747.36)	374.19 (374.27)
S	462.22 (462.27)			758.31 (758.18)	379.66	741.28	740.30	660.33 (660.36)	330.67
K	590.31 (590.27)	573.29		671.28 (671.00)	336.14	654.25	653.27	573.30 (573.27)	287.15
S	757.31	740.29 (740.27)	659.34 (659.27)	543.18	272.09	526.15	525.17	445.20 (445.27)	223.11
G	814.33 (814.27)	797.31	716.36 (716.27)	376.18 (376.27)	188.60	359.16	358.17		
D	929.36 (929.27)	912.33	831.38 (831.36)	319.16	160.08	302.13	301.15		
G	986.38 (986.09)	969.36	888.41 (888.36)	204.13 (204.09)	102.57	187.11			
K				147.11	74.06	130.09			

[M-H3PO4+2H]2+	517.73
[M-H3PO4-H2O+2H]2+	508.82

Yellow:	Out of spectrum mass range
Red:	Relative intensity >0.1
Theoretical m/z (Observed m/z)	

Suppl Table S13 for Fig S14

Cx45-29-11 #2785 @565.25 CID

S393 CID	b	b 2+	[b-NH3]	[b-NH3] 2+	[b-H3PO4]	[b-H3PO4] 2+	y	y 2+	[y-H3PO4]
S									
G	145.06						1042.46 (1042.18)	521.73 (521.73)	944.48
D	260.09 (260.00)						985.44 (985.27)	493.22 (493.18)	887.46 (887.45)
G	317.11						870.41 (870.27)	435.71	772.44 (772.55)
K	445.20 (445.27)	223.11	428.18 (428.27)	214.59			813.39 (813.27)	407.20	715.41
T	546.25	273.63	529.23	265.12			685.30 (685.09)		587.32 (587.18)
S	713.25	357.13	696.22 (696.27)	348.62 (348.73)	615.27 (615.27)	308.14	584.25		486.27 (486.27)
V	812.32 (812.27)	406.66	795.29	398.15 (398.27)	714.34 (714.27)	357.67	417.25		
W	998.40 (998.27)	499.70 (499.64)	981.37	491.19	900.42 (900.18)	450.71 (450.73)	318.18 (318.18)		
I							132.10		

[M-H3PO4+2H]2+	516.27
[M-H3PO4-H2O+2H]2+	507.18

Yellow:	Out of spectrum mass range
Red:	Relative intensity >0.2
Theoretical m/z (Observed m/z)	

Supplemental Figure S1

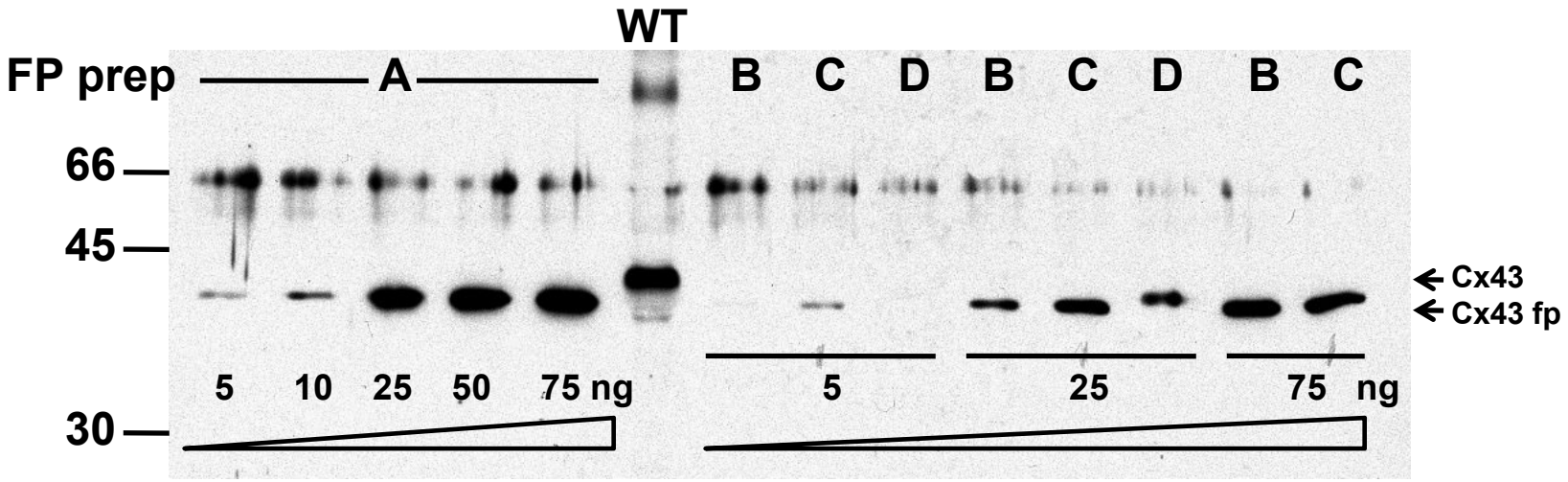

Supplemental Figure S2A

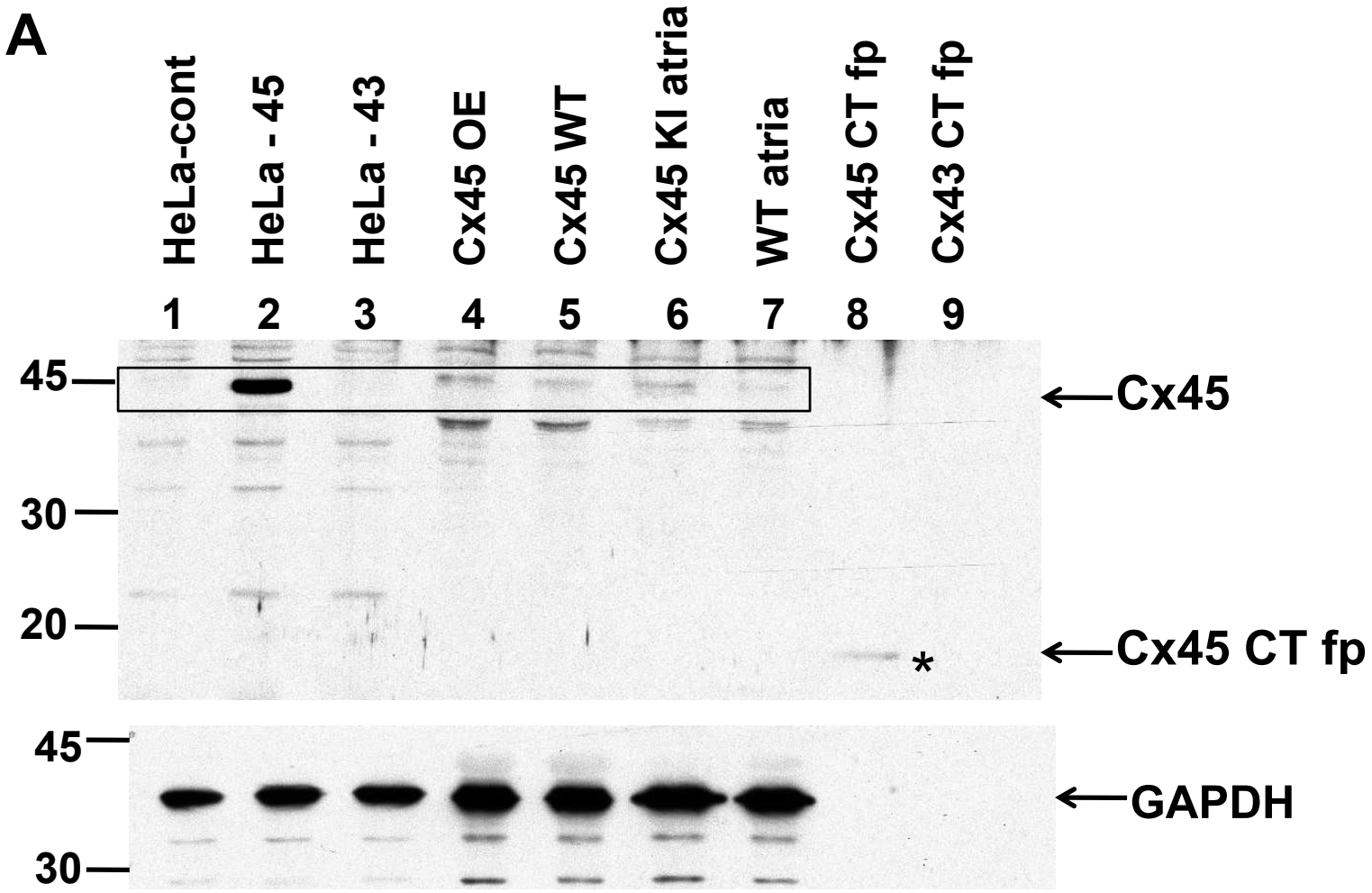

Supplemental Figure S2B

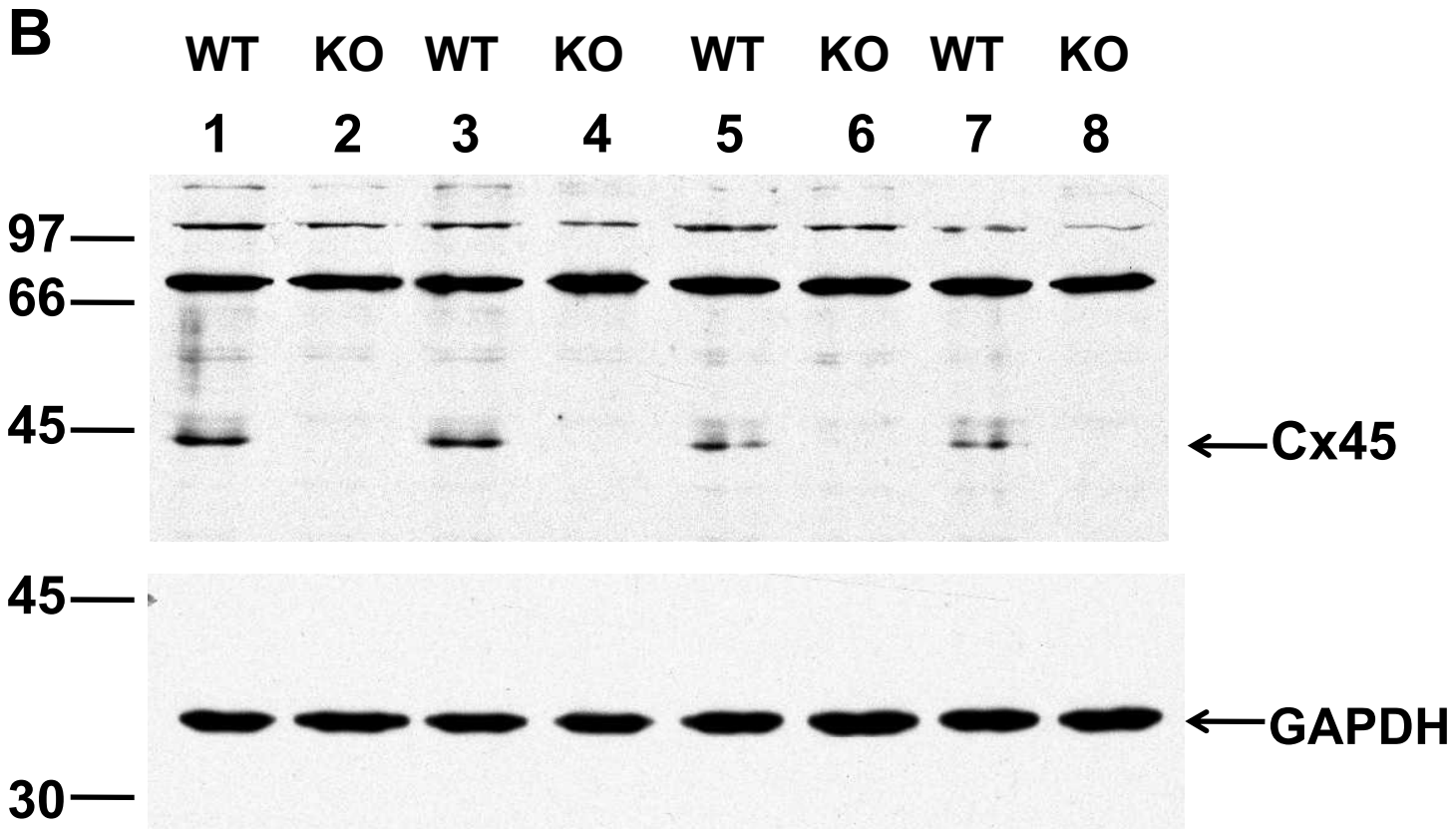

Supplemental Figure S2C

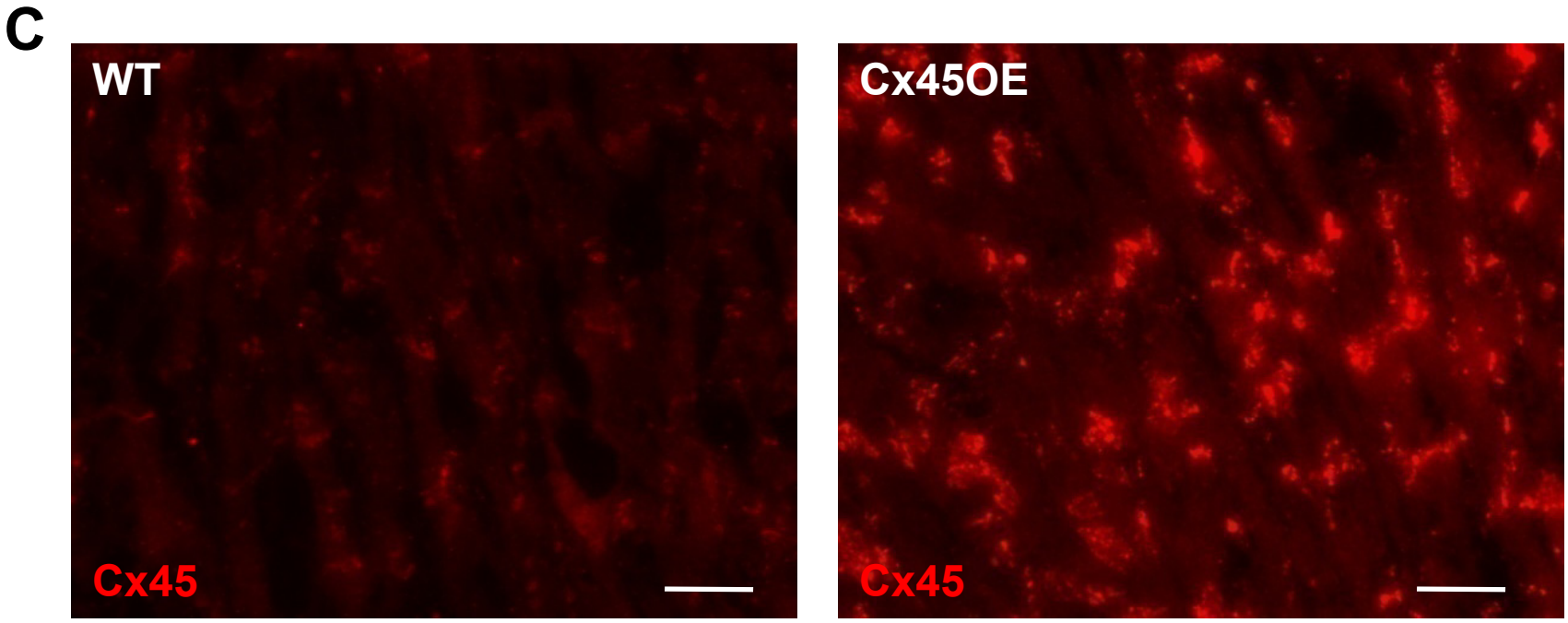

Supplemental Figure S2D

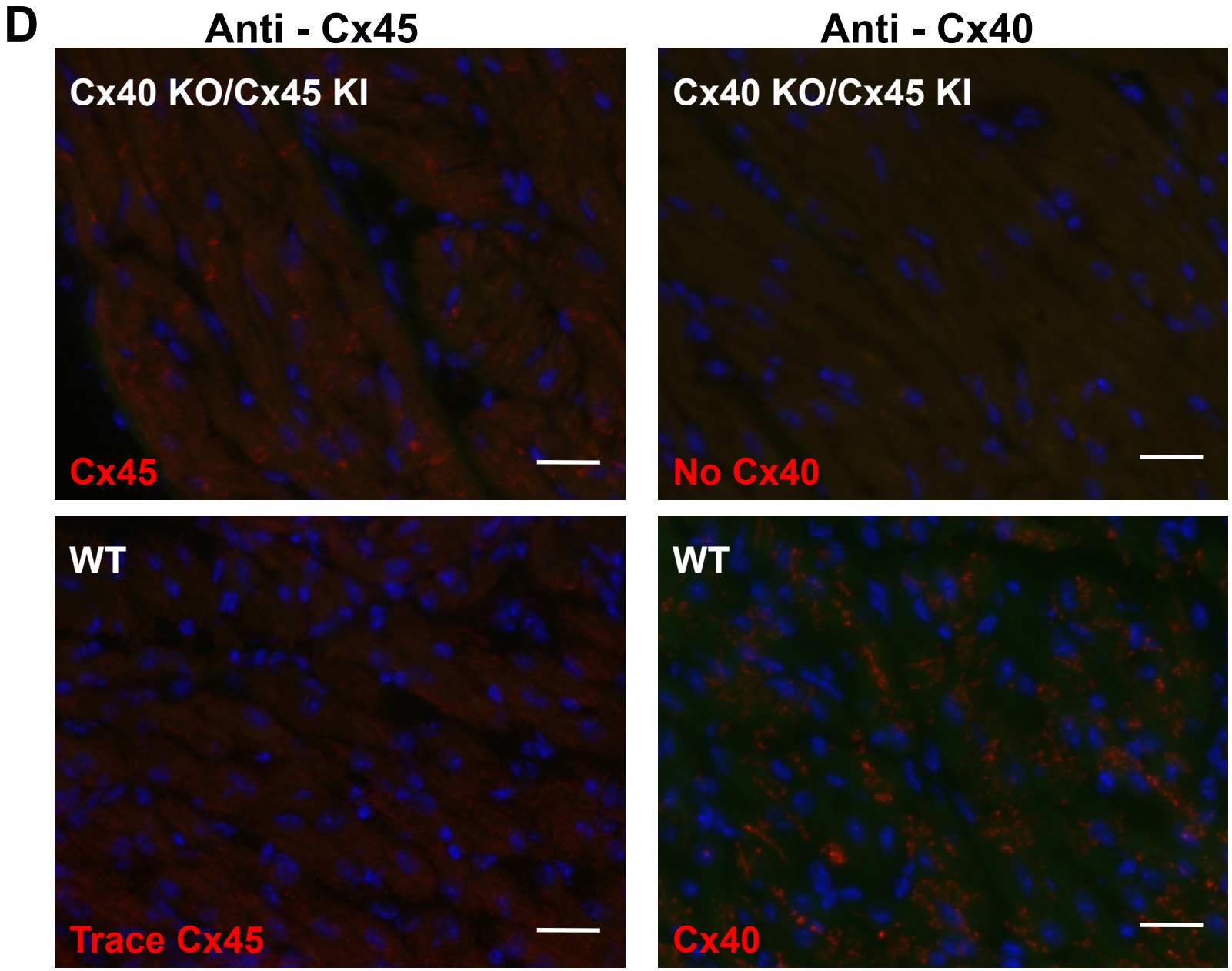

Supplemental Figure S3

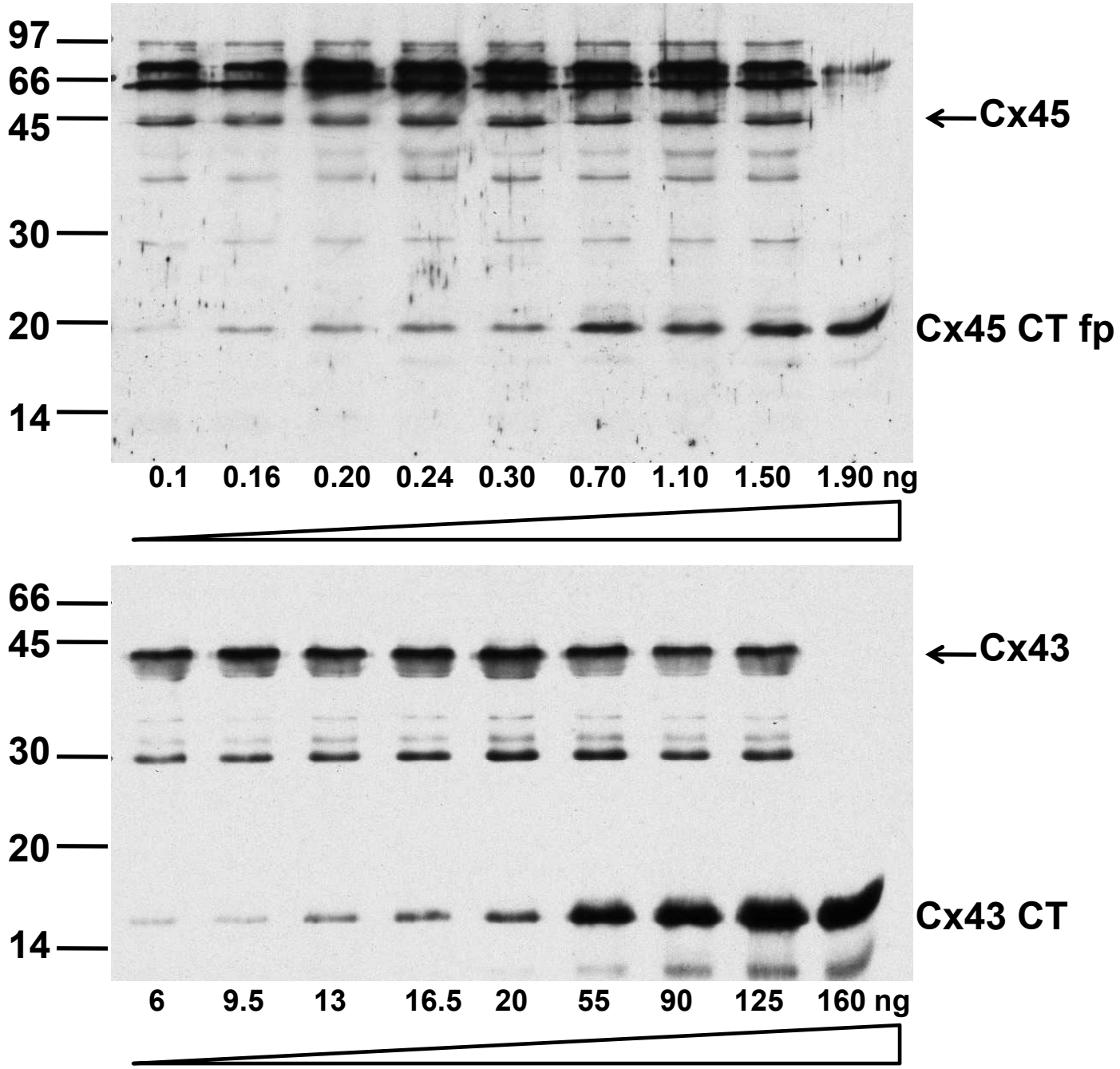

Supplemental Figure S4

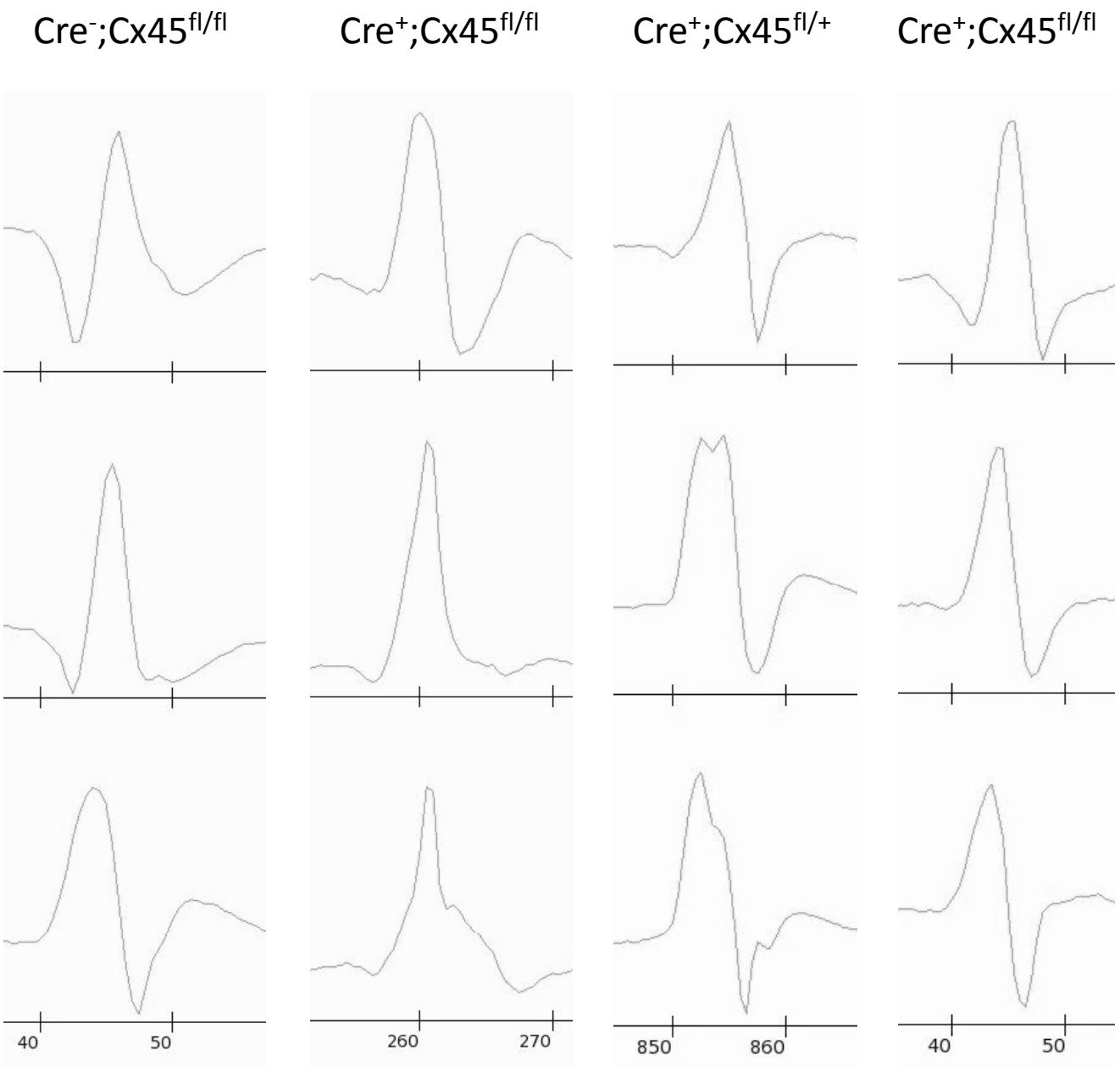

Supplemental Figure S5

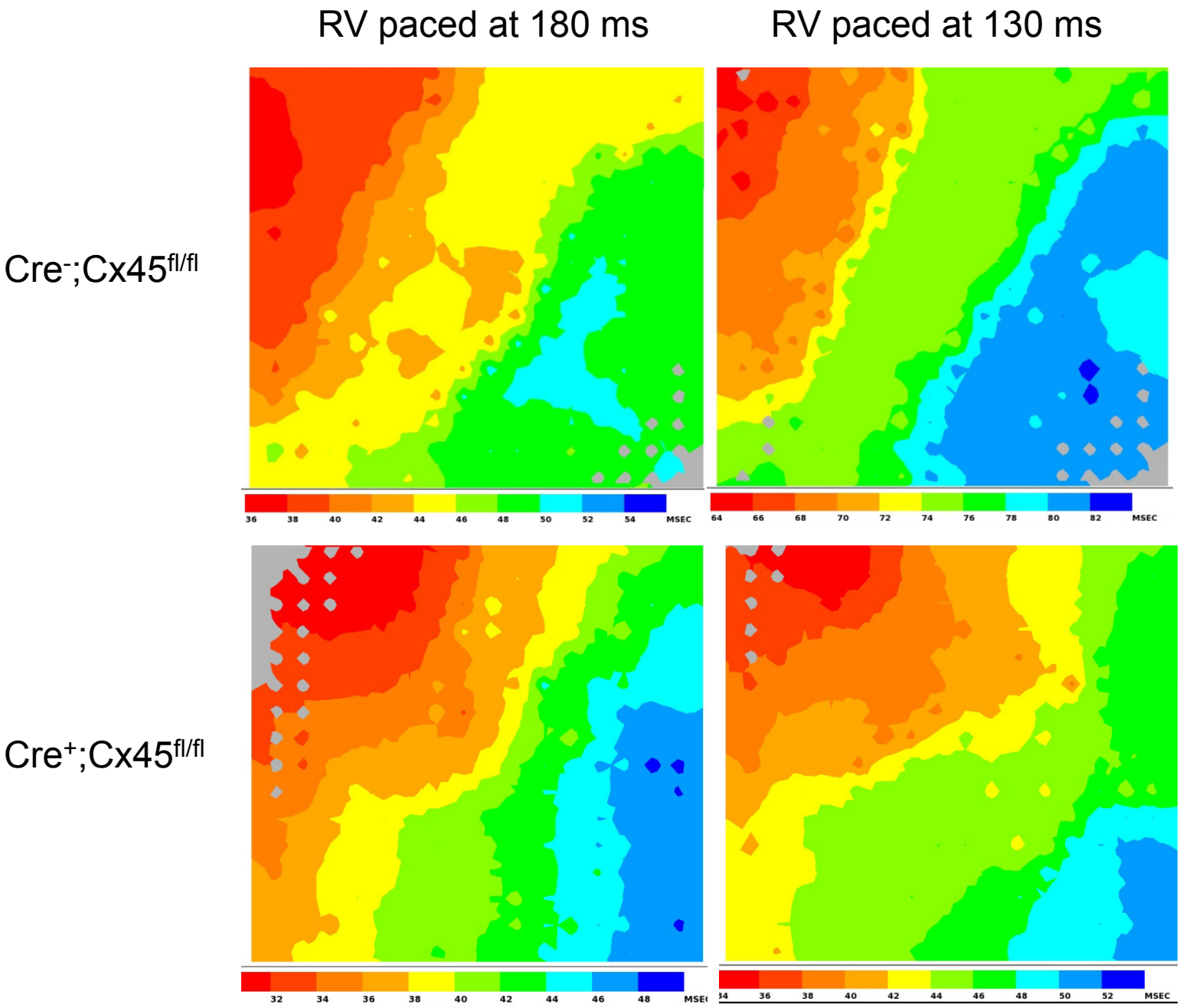

Figure S6

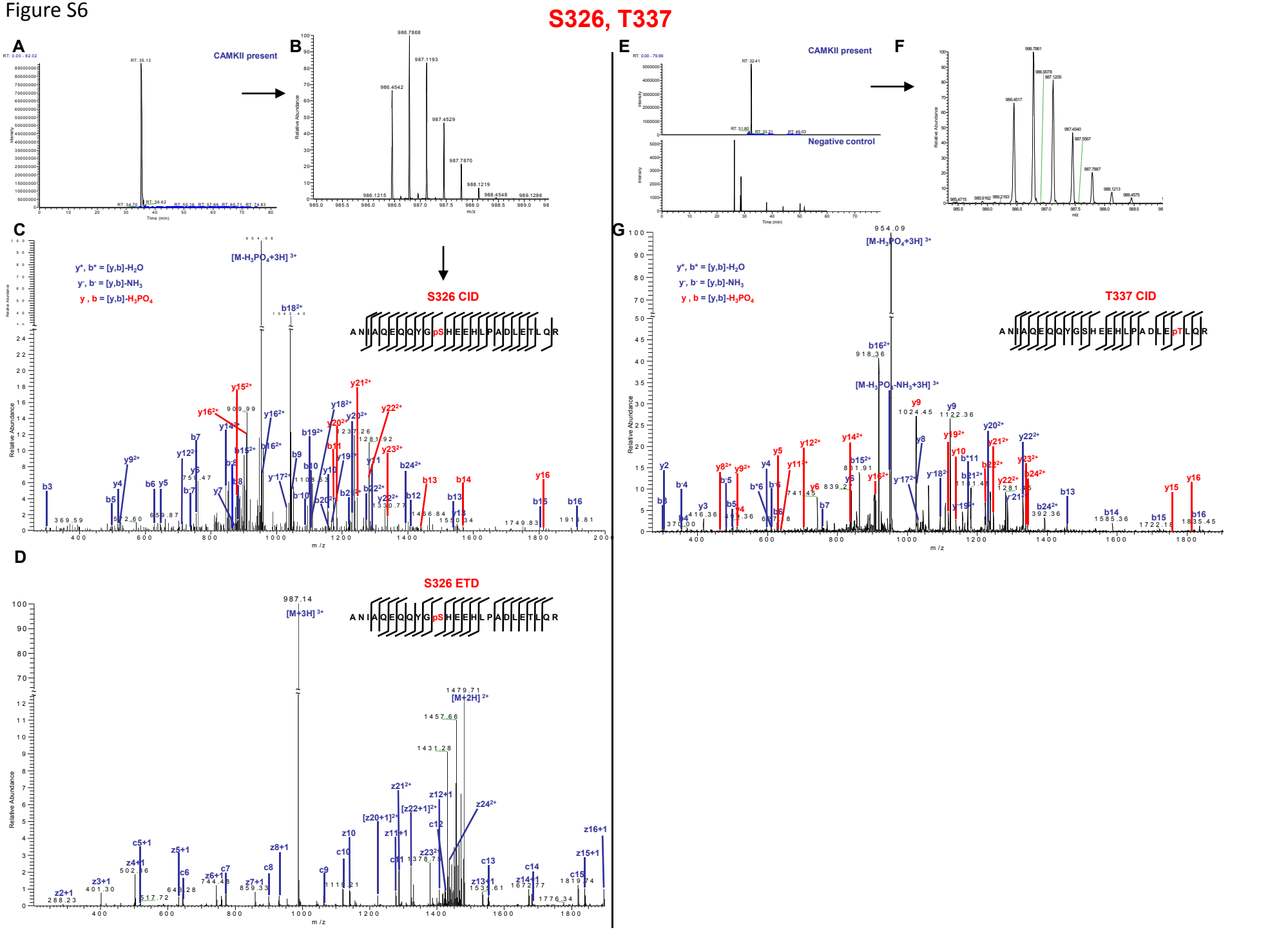
S326, T337
A
CAMKII present
B
C
y*, b* = [y,b]-H2O
y-, b- = [y,b]-NH3
y , b = [y,b]-H3PO4
[M-H3PO4+3H] 3+
S326 CID
ANIAQEQQYGpSHEEHLPADLETLQR
D
S326 ETD
987.14
[M+3H] 3+
1479.71
[M+2H] 2+
E
CAMKII present
Negative control
F
G
954.09
[M-H3PO4+3H] 3+
[M-H3PO4-NH3+3H] 3+
T337 CID
ANIAQEQQYGSHEEHLPADLEpTLQR
Relative Abundance
m/z

Figure S7

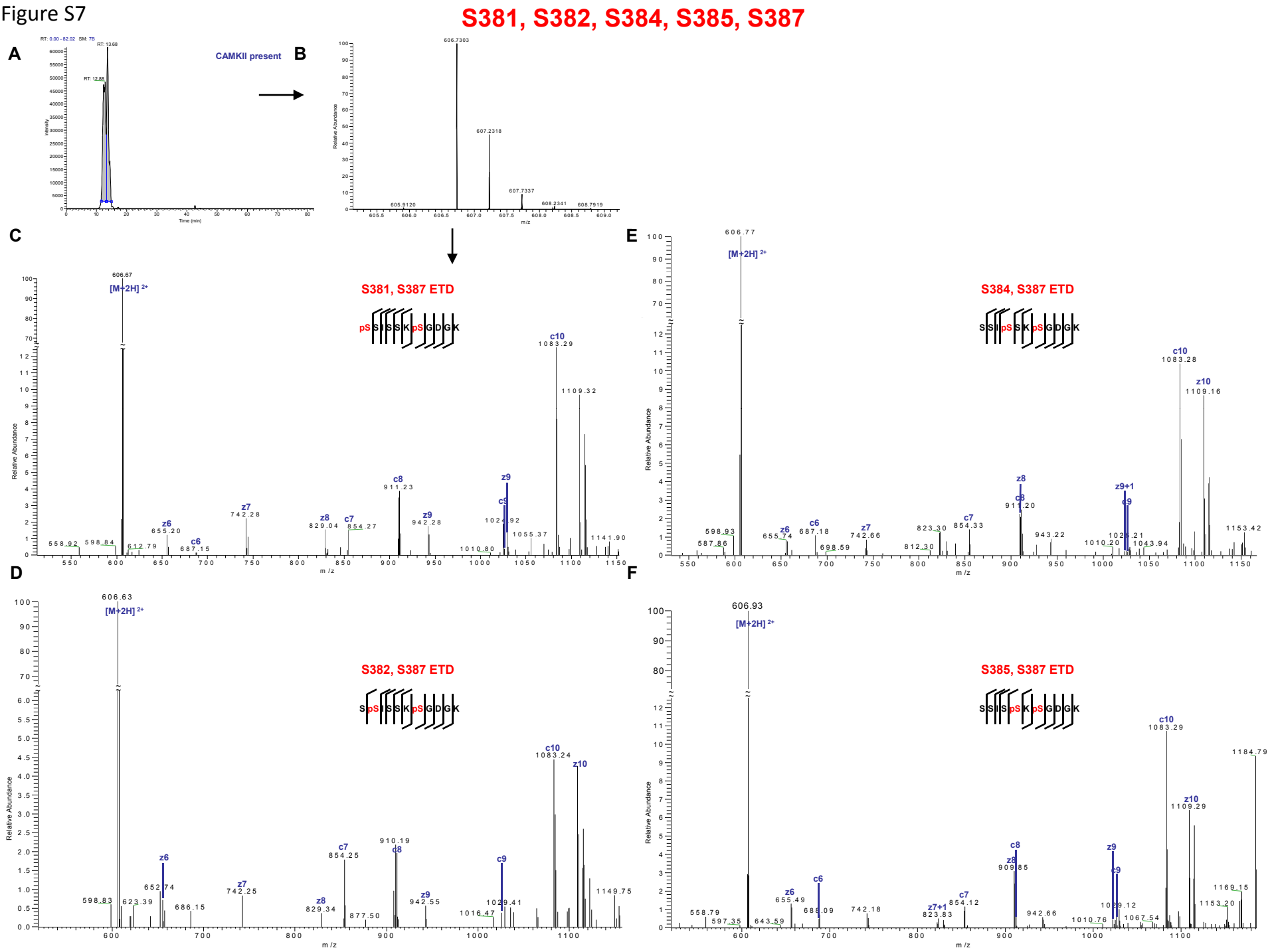
S381, S382, S384, S385, S387
A
CAMKII present
B
C
S381, S387 ETD
pSSISSKpSGDGK
[M+2H] 2+
D
S382, S387 ETD
SpSISSKpSGDGK
E
S384, S387 ETD
SSIpSKpSGDGK
F
S385, S387 ETD
SSISpSKpSGDGK
Relative Abundance
m/z

Figure S8

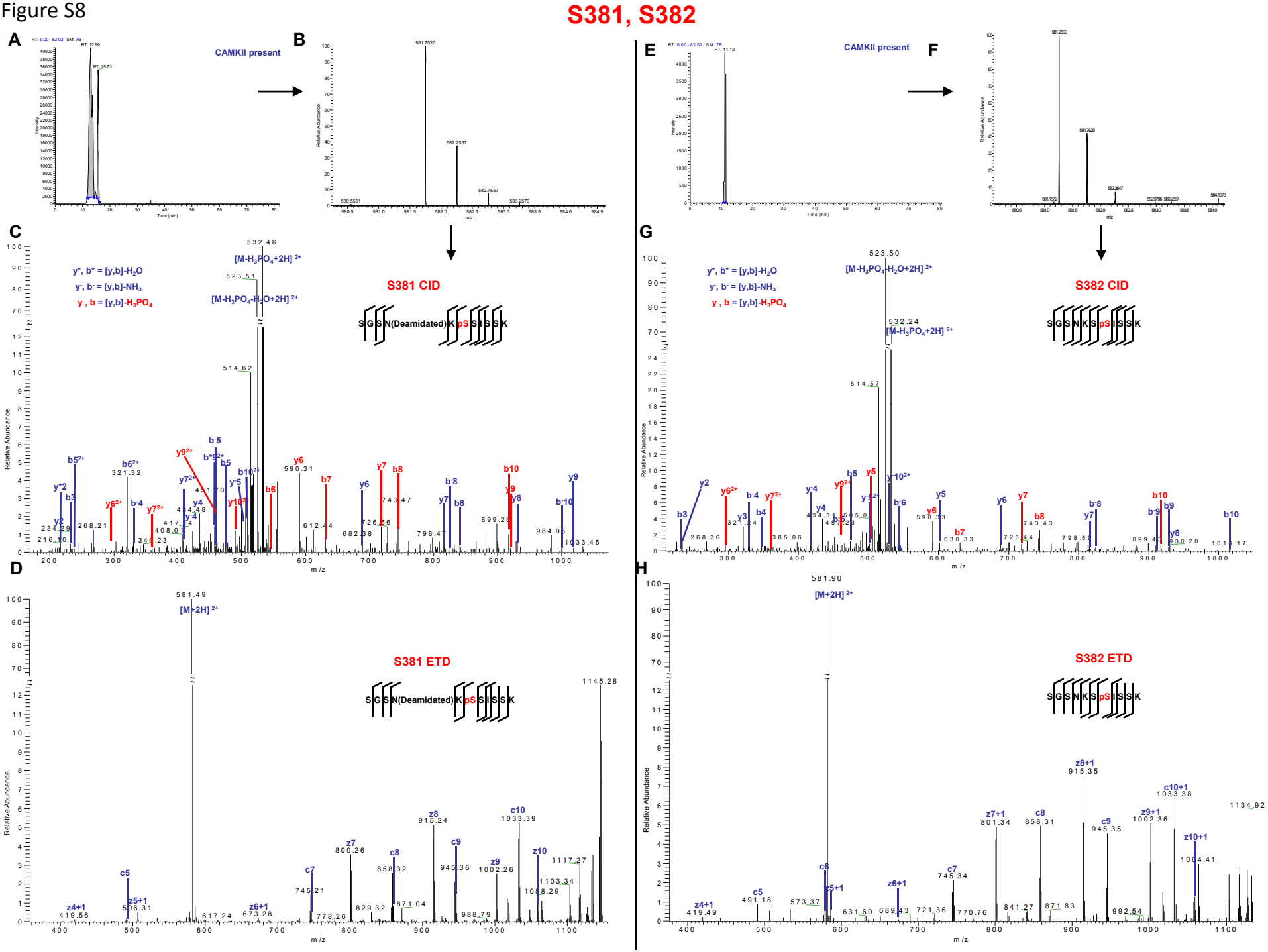
S381, S382
A
CAMKII present
B
C
S381 CID
SGSN(Deamidated)KpSSISSK
y*, b* = [y,b]-H2O
y-, b- = [y,b]-NH3
y , b = [y,b]-H3PO4
532.46
[M-H3PO4+2H] 2+
523.51
[M-H3PO4-H2O+2H] 2+
514.62
Relative Abundance
m /z
D
S381 ETD
581.49
[M+2H] 2+
1145.28
E
CAMKII present
F
G
S382 CID
SGSNKSpSISSK
523.50
[M-H3PO4-H2O+2H] 2+
532.24
[M-H3PO4+2H] 2+
514.57
H
S382 ETD
581.90
[M+2H] 2+

Figure S9

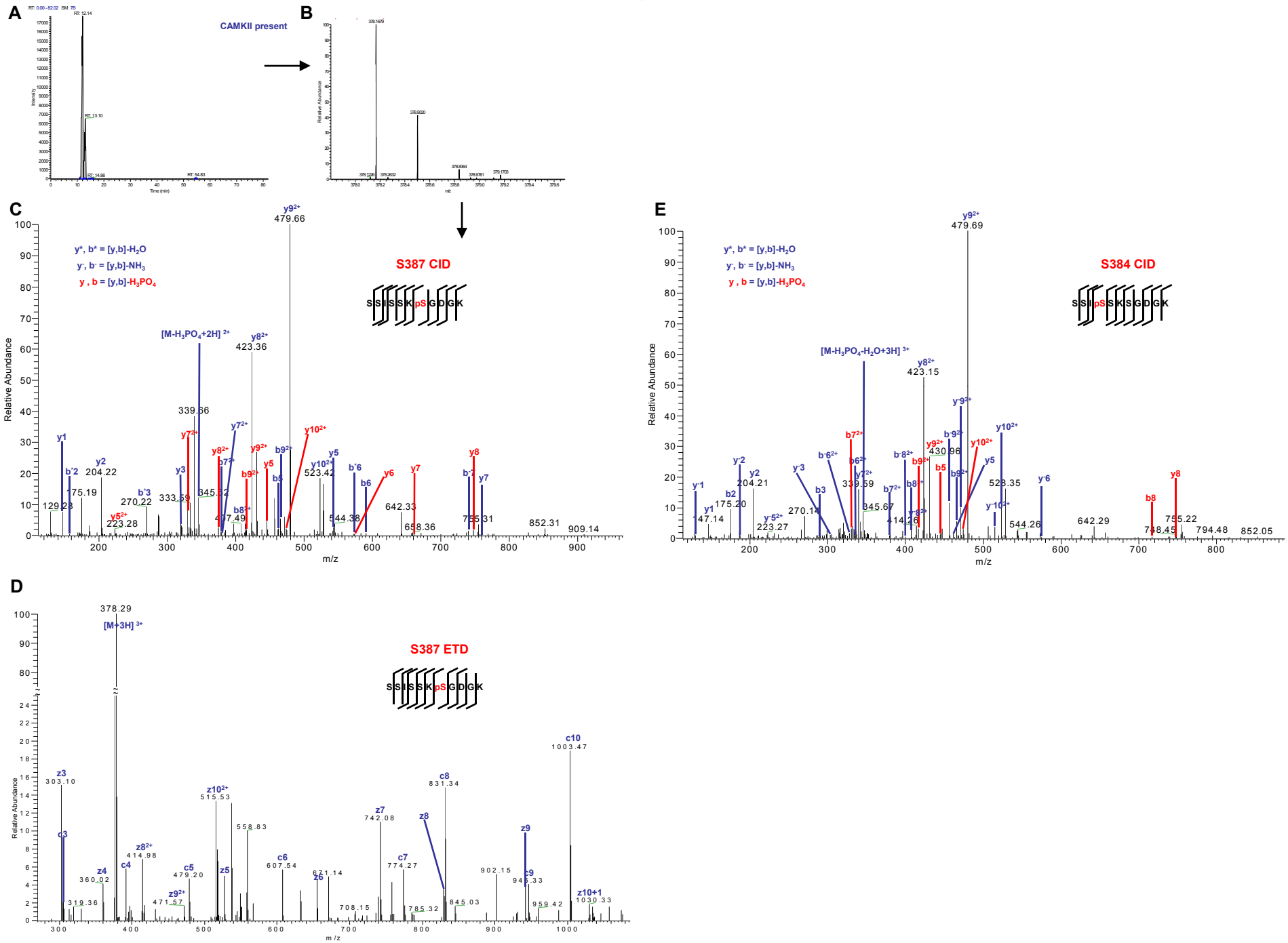
S384, S387
A
CAMKII present
B
C
S387 CID
SSIISSKpSGDGK
y*, b* = [y,b]-H2O
y-, b- = [y,b]-NH3
y , b = [y,b]-H3PO4
[M-H3PO4+2H] 2+
Relative Abundance
m/z
D
S387 ETD
[M+3H] 3+
E
S384 CID
SSIIpSSKSGDGK
[M-H3PO4-H2O+3H] 3+

Figure S10

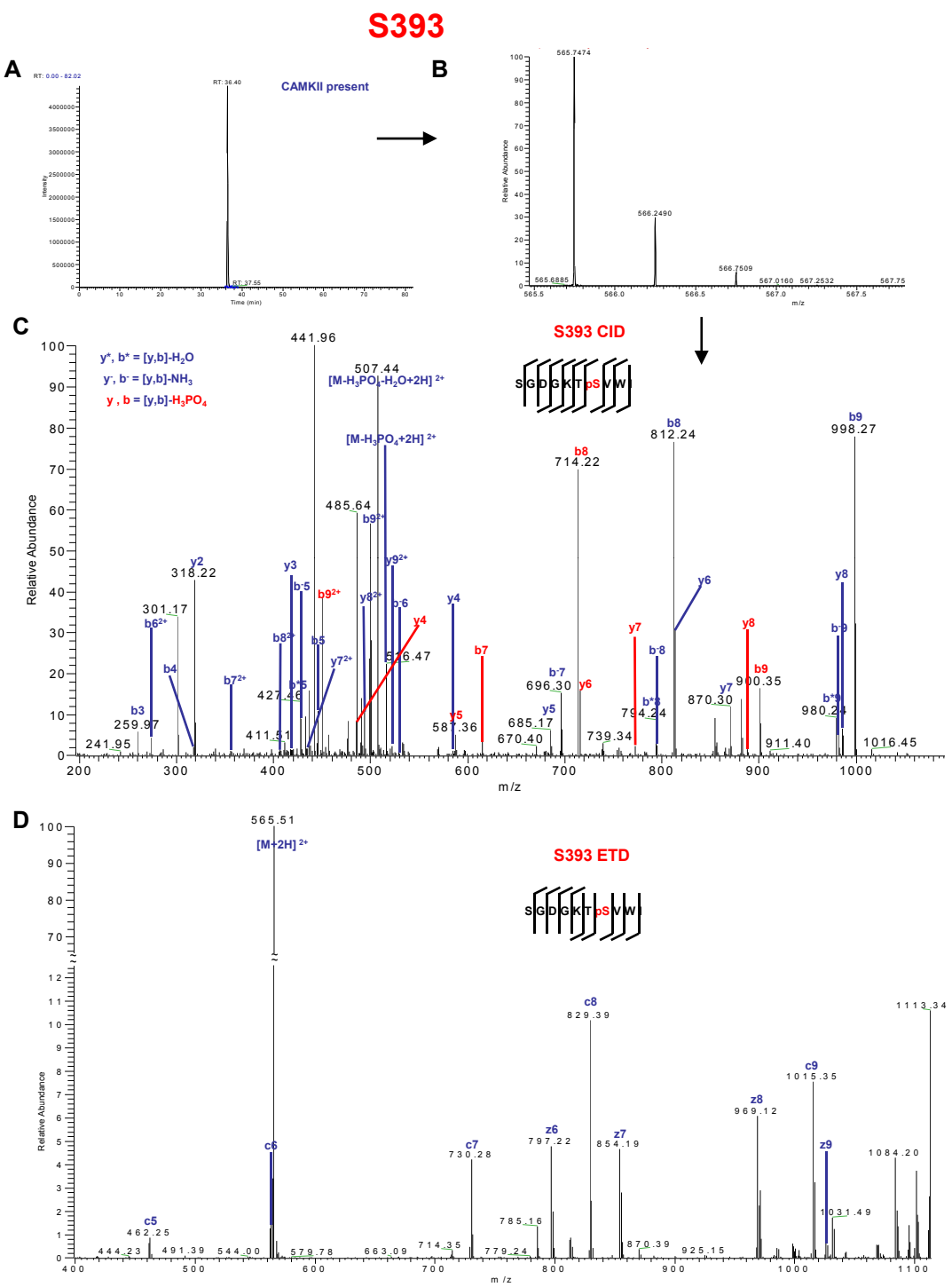
S393
A
CAMKII present
B
C
S393 CID
y*, b* = [y,b]-H2O
y-, b- = [y,b]-NH3
y , b = [y,b]-H3PO4
Relative Abundance
m/z
D
S393 ETD
Relative Abundance
m/z

Figure S11

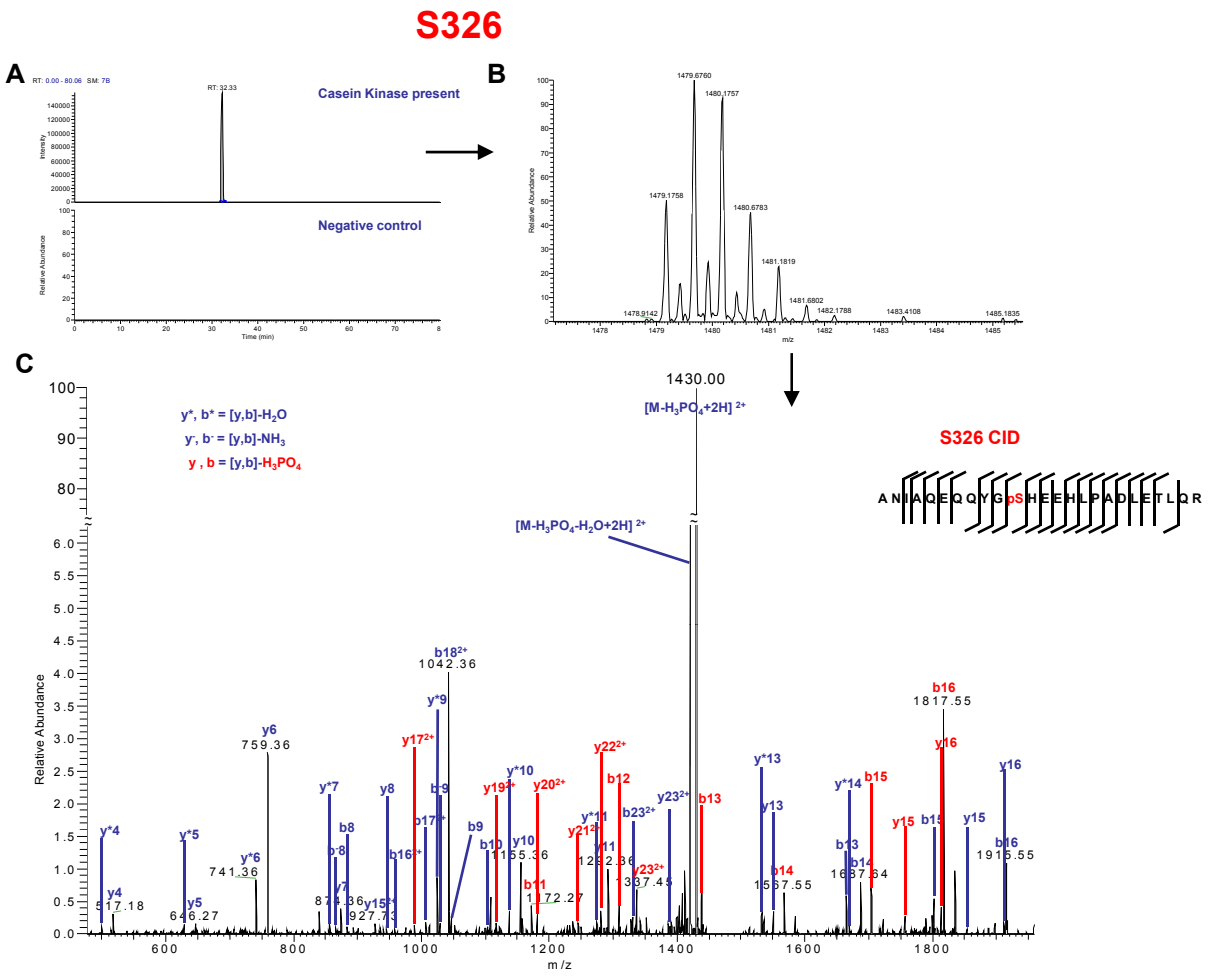
S326
A
Casein Kinase present
Negative control
B
C
1430.00
[M-H3PO4+2H] 2+
[M-H3PO4-H2O+2H] 2+
y*, b* = [y,b]-H2O
y-, b- = [y,b]-NH3
y , b = [y,b]-H3PO4
S326 CID
ANIAQEQQYGpSHEEHLPADLETLQR
Relative Abundance
m/z

Figure S12

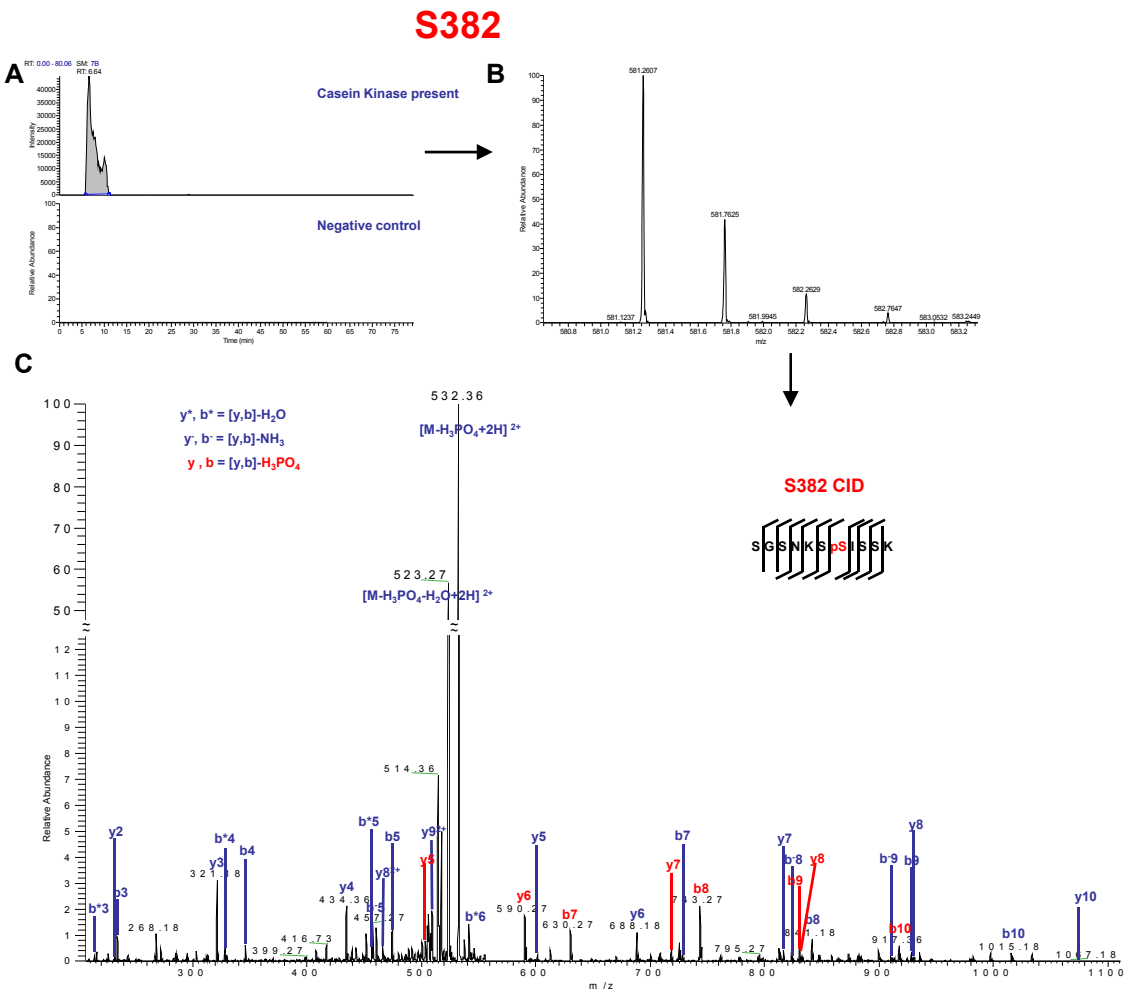
S382
A
Casein Kinase present
Negative control
B
C
y*, b* = [y,b]-H2O
y-, b- = [y,b]-NH3
y , b = [y,b]-H3PO4
532.36
[M-H3PO4+2H] 2+
523.27
[M-H3PO4-H2O+2H] 2+
S382 CID
SGSNKSpSISSK
Relative Abundance
m/z

Figure S13

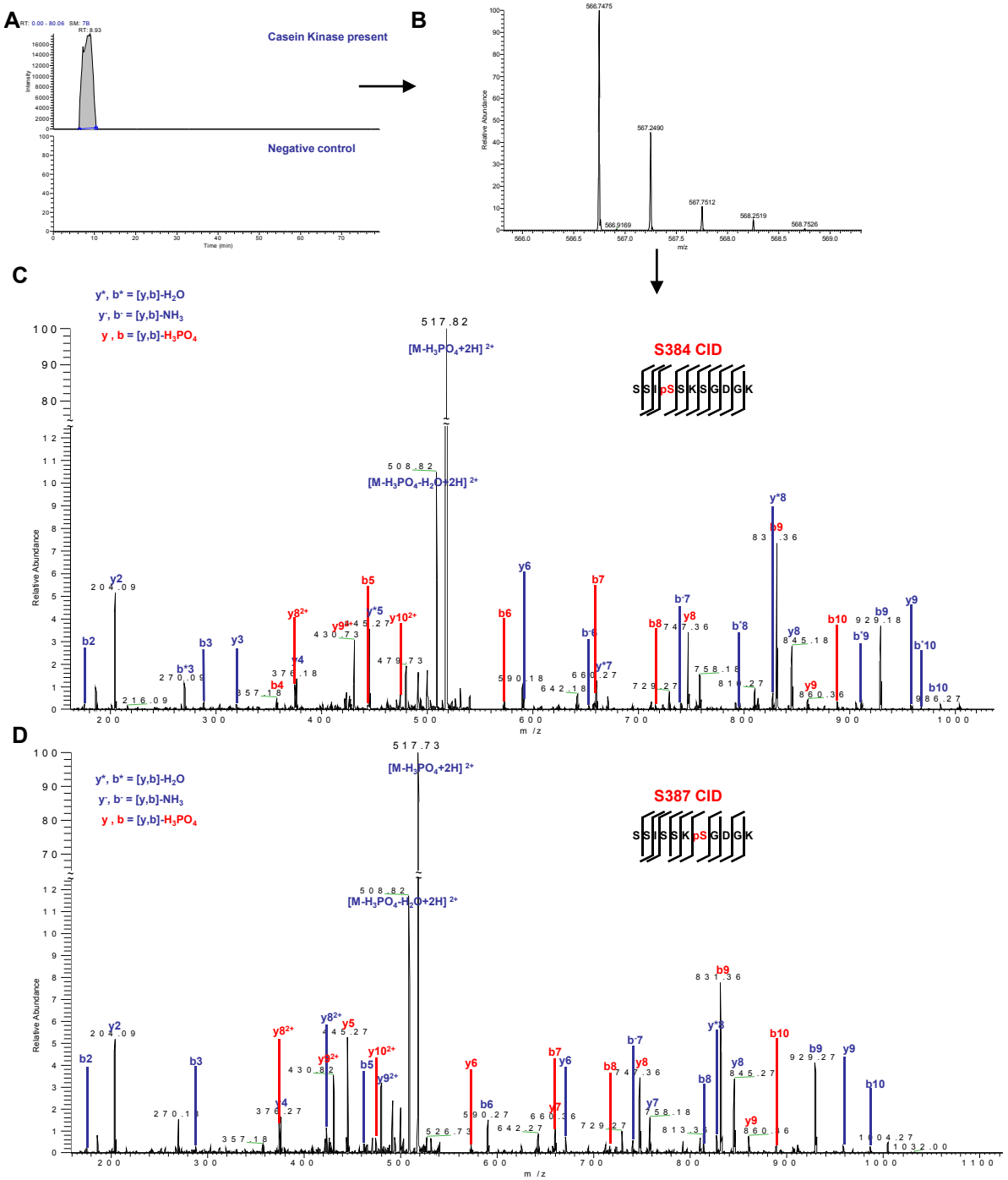
S384, S387
A
Casein Kinase present
Negative control
B
C
y*, b* = [y,b]-H2O
y-, b- = [y,b]-NH3
y , b = [y,b]-H3PO4
517.82
[M-H3PO4+2H] 2+
S384 CID
SSIpSSKSGDGK
508.82
[M-H3PO4-H2O+2H] 2+
Relative Abundance
m /z
D
y*, b* = [y,b]-H2O
y-, b- = [y,b]-NH3
y , b = [y,b]-H3PO4
517.73
[M-H3PO4+2H] 2+
S387 CID
SSISSKpSGDGK
508.82
[M-H3PO4-H2O+2H] 2+
Relative Abundance
m /z

Figure S14

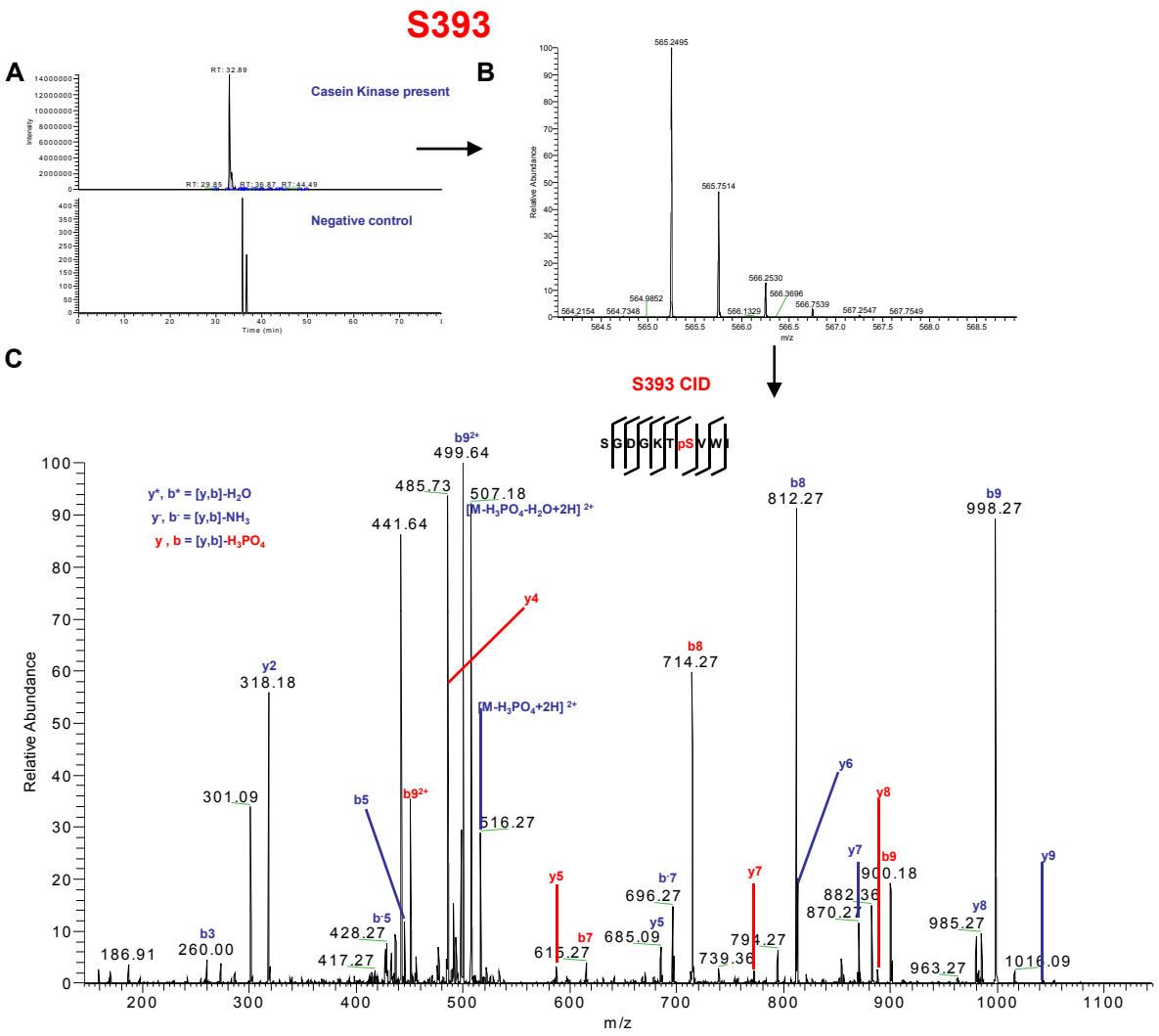
S393
A
Casein Kinase present
Negative control
B
C
S393 CID
SGDGKTpSVWI
y*, b* = [y,b]-H2O
y, b = [y,b]-NH3
y , b = [y,b]-H3PO4
[M-H3PO4-H2O+2H] 2+
[M-H3PO4+2H] 2+
Relative Abundance
m/z